Study on oscillation characteristics of a spar-buoy under Mathieu instability

Doctoral Dissertation

STUDY ON OSCILLATION CHARACTERISTICS OF A SPAR-BUOY UNDER MATHIEU INSTABILITY

MARCH 2020

Graduate School of Marine Science and Technology
Tokyo University of Marine Science and Technology
Doctoral Course of Applied Marine Environmental Studies

XU PENG

Contents

Abstract

With the rapid development of human society, the demand for energy is growing rapidly. Energy is the foundation of economic development and a material guarantee for improving the quality of human life. Since the industrial revolution, the transitional consumption of traditional fossil energy has brought about energy shortages and environmental pollution. Since the first oil crisis in 1973, people have paid more and more attention to the development of renewable resources. For the sustainable development of human beings, it is of importance to adjust the energy structure and discovery of renewable energy. In recent years, renewable energy sources, such as wind energy and solar energy, have been put into much attention, and related applications have also been promoted. Although wave energy is another form of renewable and clean energy, it has not been widely promoted like wind and solar energy. Wave energy is potential energy with the advantages of no pollution and wide distribution. As an excellent renewable energy, ocean energy is inexhaustible. Marine energy accounts for about 70% of the global total energy. If fully utilized, it will greatly alleviate current energy shortages.

Due to its advantages, the high energy flux density, rarely limited by time, available to implement wave power for power generation and supply with smaller volume, wave energy has attracted more and more interest from scholars and researchers around the world. Waves energy extraction is achieved by using the device called Wave Energy Converters (WECs), which convert wave power into electricity. Over the last few decades, large number of WECs have been developed, tested and presented in publications. According to the working principle, the technologies could be classified into three main types: the oscillating water column, the over-topping and the oscillating bodies. One of the most typical oscillating bodies is point absorbers, which can harness incoming wave-energy from all directions with the normal function in most of the time and keep relatively small size and simple functional principles with relative lower cost.

WECs technologies are still in its infant stage, which naturally confronts this renewable energy converters with lots of challenges, problems and barriers during its maturation. To maximize the waves energy, the oscillation characteristics of the floating device, such as point absorbers, should be optimized to the most frequent waves at the local site. However, the bandwidth of the frequency response is relatively narrow, and the natural frequency is much higher than the typical ocean wave frequencies. Therefore, several methods of phase-control have been proposed and carried out. Meanwhile, it is well known that the spar-type platform shows extreme heave motion at resonance. Moreover, parametric resonance of the pitch motion has been confirmed. When the frequency of the heave motion is approximately twice the pitch natural frequency, the very large amplitude

oscillatory motion will occur.

By changing the viewpoint, a new concept was proposed to utilize the Mathieu-type instability for WECs. A subject was carried out and limited to pure heave motion of a spar-buoy type point absorber and utilized the Mathieu-type instability by the dynamic buoyancy control system. However, it was also revealed that the efficiency was far from practical applications. As the improvement of the study, the subject was focused on a coupled motion of heave and pitch.

The research work of this thesis mainly consists of four parts, one part includes the experimental work and other three parts are the analysis work based on the experimental results. And the contents are organized as follows:

In the first part, the experimental devices were designed and made. A ballast controlling system into the buoy was installed to change the natural frequency of the pitch motion. The free decay of buoy damping motion was carried out to make the buoy model satisfy the Mathieu instability condition (the natural frequency of heave is double the natural frequency of pitch motion). After that, the experiment was carried out with regular wave. Based on the experiment results, it is indicated that the large pitch motions occur suddenly and the heave amplitude shrinks just after the occurrence of larger pitch motion.

In the second part, it aims to investigate existence of the energy transform of the buoy motions. The signals of the heave acceleration were integrated with high pass filtering in the frequency domain and the vertical velocities and displacements of the buoy were calculated. Base on the integrated data and the original measured data, the kinetic and potential energy of heave and pitch motions were calculated. The energy transform of the buoy motions is discussed in time domain. The total energy takes the maximum value around 16s and the first half of the peak is dominated by the heave energy and the latter half is replaced by the pitch energy. Therefore, this can be concluded that the energy was transferred from the heave mode to the pitch mode and shrunken by the pitch damping. On the other hand, the power to be taken off is closely related to the total energy.

In the third part, in order to find some conditions in which the large pitch motion occurs suddenly by considering the theoretical condition of the Mathieu-type instability. The righting lever of the buoy model is calculated with assuming the free board is infinite. The relationship between the pitch angle and the righting lever under the Mathieu-type instability was theoretically discussed in the time domain. It was indicated that the experimental relationship between the pitch angle and the righting lever during the large pitch motions is similar to the theoretical characteristic of the Mathieu-type instability. The large pitch motion disappears just after the theoretical characteristic of the Mathieu-type instability is lost.

In the last Part, the occurrence of the large pitch motion is investigated by the stability chart

of the Mathieu equation. The stability chart of Mathieu equation was plotted for the experiment with the method of the harmonic balance. It could be found that all the experimental results were in the unstable region before the large pitch motion disappeared, which induced the Mathieu-type instability of pitch motion. Before the large pitch motion decayed, the stability results were in the stable region of the stability chart of Mathieu equation. It was shown that the large pitch motions disappeared (decayed) at the timing when the condition of the Mathieu-type instability is lost. It has been shown stability results returned to the unstable region, and large pitch motion occurred again after large pitch motion disappeared, which is induced by the condition of Mathieu instability.

Keywords: Point absorbers; Coupled motions; Mathieu instability; Energy transfer; Righting lever; Stability analysis; Power generation efficiency

Chapter1 Introduction

1.1 Background

The energy services are necessary for all societies to satisfy basic human needs and to serve process of production. For over a century, most of the used electricity that has been generated in large power plants is from fossil fuels, nuclear reactor and hydroelectric turbine. Taking account of the climate change, environmental disruption, overconsumption of fossil fuel and risks of nuclear power, terms such as *renewable*, *sustainable* and *carbon-free* become a hot issue for considering the method of electricity generating. [1-3] The fossil fuels on earth is not inexhaustible. Most experts and politicians in every country across the world have advocated and made the concerned policies for the sustainable development, especially with regards to lose environmental impacts and low greenhouse gas (GHG) emissions. However, based on IPCC Fourth Assessment Report (AR4), it is shown that 85% of the total primary energy is provided by fossil fuels and 56.6% of all anthropogenic GHG emissions came from the combustion of fossil fuels accounted in 2004. [4,5]

In the face the pressure of the shortage of non-renewable energy, countries around the world have begun to attach importance to the development of renewable energy and the rational use of non-renewable energy. On the one hand, people pay more attention to energy conservation and sustainable energy development; On the other hand, all countries attach great importance to the development and utilization of new energy sources, such as wind energy, ocean energy, ammonia energy, geothermal energy, and so on. As an excellent renewable energy, ocean energy is inexhaustible and has received widespread attention. Marine energy accounts for about 70% of the global total energy, and it will greatly alleviate the current energy shortage problem if being fully exploited. [6]

The renewable marine (ocean) energy comes includes six distinct sources: waves, tidal range, tidal currents, ocean currents, ocean thermal energy conversion and salinity gradients. [7] According to statistics, the theoretical renewable power of global marine energy is about 7.66 x 10^{10} kW, but it cannot be fully developed and utilized by humans. In the actual marine energy that is available for humans, wave energy is the largest, about 3×10^{8}kW. The energy density of wind is 0.4~0.6 kw/m and the energy density of solar is 0.1~0.2 kw/m, compared with which, the energy density of wave energy is largest, up to 2~3kw/m. [8,9] Hence, wave energy is an intermittent energy source and widely considered as one of the most alternative renewable and sustainable energy. In the ocean engineering, it is one of the most attractive research to convert wave energy to the electricity and many types of the energy-extracting technologies have been developed and some full-scale devices were built. [8,10,11]

Now, however, harnessing of wave energy is far from being put into commercial application. Waves energy extraction is achieved by using the device called Wave Energy Converters (WEC). One of the most several challenges that WECs have to obstacle is that most of wave energy just can be captured and utilized offshore, which increases the costs of power transferred to the grid and maintenance. In addition, the tremendous potential of wave energy has increased the motivation for continued research. As offshore activities are almost inevitable, researchers take focus on studying and producing much more efficient wave energy extraction methods. [12] Optimization of WECs can realize much more economic waves energy conversion in the future.

1.2 Wave energy technologies

WECs can convert wave power into electricity, the technologies of which vary wildly in the mechanical and electrical principal of operation. Over the last few decades, large number of WECs have been developed, tested and presented in publications. [13] According to the working principle, in Figure 1.1, the technologies could be classified into three main type as shown:

a. the oscillating water columns (OWC)

OWC is a partially submerged enclosed structure, the upper part of which is above the water and is mainly composed of a closed air chamber. The incoming waves are emptied to the bottom part of the structure. With these waves coming through the structure, the water column that rises and falls in response to the pressure from the ocean waves, which drives air through a wind turbine and the turbine drives a generator for electricity production to converter the energy [14,15], see Figure 1.1(a).

b. the over-topping

The principle of the over-topping wave energy generating device is to convert wave kinetic energy into water potential energy and then to electrical energy. Overtopping device is partially submerged. The wave crosses the top of the ramp into the device's reservoir and kinetic energy of the waves is converted into potential energy. The water backs into the ocean from the reservoir through water turbines, thus utilizing the potential difference between the ocean and the reservoir to generate electricity[15], see Figure 1.1(b).

c. The oscillating bodies

The WEC's structure of oscillating bodies are floating or (more rarely) fully submerged. The devices produce the motion response to the ocean waves, and kinetic energy is harnessed and converted to electricity. [8, 17,18] One of the most typical is point absorbers, se Figure 1.1(c).

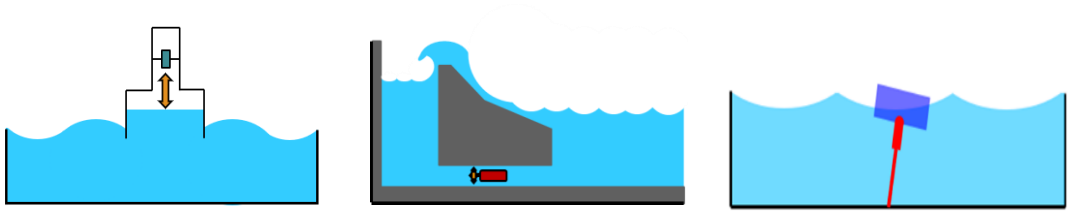

(a) *The oscillating water column* (b) *The over-topping* (c) *The oscillating bodies*

Figure 1.1 Wave energy converters

Point absorbers are usually smaller than other WECs. The classical point absorbers are equipped with floating parts which can capture the kinetic energy from wave-induced motions. Point absorbers are designed to be attached to the seabed via pillar or cable. A Power Take Off device (PTO) is placed somewhere between the seabed and the floater and it can convert the mechanics into electricity [19,20]. Compared with other types of WECs, point absorbers keep special advantages [12,21]:

1) Point absorbers are capable of harness incoming wave-energy from all directions and keep the normal function in most of the time unless extreme wave conditions occur;
2) The designment of point absorbers is not so difficult, and they keep relatively small size and simple functional principles. Hence, they could be more cost-effective, on account of manufacturing, installation and maintenance.

Based on above advantages, this research on WECs focusses on point absorbers.

1.3 Optimization of point absorbers

To maximize the waves energy, the oscillation characteristics of the floating device, such as point absorbers, should be optimized to the most frequent waves at the local site. However, the bandwidth of the frequency response is relatively narrow, and the natural frequency is much higher than the typical ocean wave frequencies. Therefore, several methods of phase-control have been proposed and carried out. [22-29] One of the prominent measures to improve the efficiency is phase control by latching, and which optimization method already been analyzed and carried out in the practicality. [30-33]

On the other hand, it is well known that the spar-type platform shows extreme heave motions at resonance. Moreover, parametric resonance of the pitch motion has been confirmed. When the frequency of the heave motion is approximately twice the pitch natural frequency, the very large amplitude oscillatory motion will occur. In this case, it is essential to analyze the motions from the viewpoint of Mathieu-type instability and the preventive measures should be investigated. [34~39]

By changing the viewpoint, a new concept was proposed by Iseki[40,41] to utilize the Mathieu-

type instability for WEC. As a first step, the subject was limited to pure heave motion of a spar-buoy type point absorber. Theoretically, it is well known that the auto-parametrically excited oscillation based on the Mathieu equation can be induced by the fluctuating restoring force. A possible measure to control the restoring force is alteration of the water plane area. For that purpose, an investigated spar-buoy model was surrounded by outer cylinders which airtightness was controlled by axially sliding valves. Based on the numerical simulations, the possibility of utilization of auto-parametrically excited oscillation was shown but the subsequent model experiments revealed that the axial sliding valves were insufficient to induce an auto-parametrically excited oscillation.

Iseki[42] developed another control system (axial sliding valves) that consists of movable floating columns and a step motor, which can realize the dynamic buoyancy control. Base on the result of model tests, it was confirmed that the dynamic buoyancy control system could utilize the Mathieu-type instability. However, it was also revealed that the efficiency was far from practical applications because the system required some amount of energy to drive itself. Therefore, it was concluded that the controlling energy haves to be supplied from the oscillating response itself like the parametric rolling in order to induce a real auto-parametrically excited oscillation.

As the extension and continuation of the study, Xu and Iseki [43] proposed a subject that was focused on a coupled motion of heave and pitch. A new spar buoy model with innovative ballast control system was made. The system is installed in the buoy model and the vertical movement of the ballast produces a certain change of the pitch natural period. In this research, the system is not controlled dynamically but used to realize several initial conditions efficiently. Based on the conducted model experiments, it was shown that the large oscillatory motion based on the Mathieu-type instability could be realized.

Iseki and Xu [44] discussed the experimental relationship between the pitch angle and the righting lever during the large pitch motions, which is similar with the theoretical characteristic of the Mathieu-type instability. It also was shown that the large pitch motion disappeared just after the theoretical characteristic of the Mathieu-type instability is lost and the Mathieu-type instability can be induced by controlling the phase relation between the pitch and heave motions.

During the experiment, it can be observed that the large pitch motion occurred suddenly and decayed at a short time, after which large pitch motion occurred again. In order to explain this phenomenon, Xu and Iseki[45] plotted the stability chart of Mathieu equation for experimental results with the method of the harmonic balance. It has been indicated that the large pitch motions disappeared (decayed) at the timing when the condition of the Mathieu-type instability is lost. It has been shown stability results returned to the unstable region, and large pitch motion occurred again after large pitch motion disappeared, which is induced by the condition of Mathieu instability.

1.4 The objectives of research

Wave energy is an intermittent energy source, which is widely considered as one of the most alternative renewable and sustainable energy. WECs technologies are still in its infant stage, which naturally confronts this renewable energy converters with lots of challenges, problems and barriers during its maturation. To maximize the waves energy and realize the large oscillation of the buoy, the purpose of this research is to improve the efficiency by using parametric self-excited oscillation of WECs. The study focuses on the coupled motion of a spar-buoy type point absorber with coupled motion (heave and pitch), and the buoy is equipped with a ballast control system to generate parametric self-excited oscillation based on Matthew-type instability. A spar-buoy type was made of and the ballast control system was installed into the model. The ballast control system can control the natural period of pitch motion by the vertical moving of the ballast. With using this buoy model, the measurement experiment was carried out in a regular wave. As a result, a phenomenon that the large pitch motions occur suddenly. The kinetic energy of the large pitch motion seems to be supplied from the heave motion. Based the righting level in time domain and stability chart of Mathieu equation, the occurring of large coupled motions can be analyzed and proved with the theory of Mathieu instability.

The main intention of the research is how to continue and keep large kinetic energy occur continuously. According to the experimental results, the large pitch motions disappearing at the timing is regarded as the buoy losing the condition of the Mathieu-type instability. The concrete restoring coefficient δ depends on the natural frequency of pitch motion ω_{np} and the natural frequency of heave motion ω_{nh}. Before Mathieu instability condition disappears, it is possible increase the natural frequency of pitch motion or decrease the natural frequency of the heave motion to be capable of keeping the value of (δ, ε) always in the unstable region based on stability chart of Mathieu equation. Then the large motion of buoy will occur continuously. The continuous large kinetic energy can improve the kinetic energy up to 3-5 times with frequency control, compared with the no control of natural frequency. This is very useful to be applied to the designment of WECs. The large kinetic energy can be transformed to the electricity. Power generation efficiency of renewable energy can be improved, which contributes to the development of human society.

Chapter2 Theory

2.1 Introduction

In this section, in order to analyze the characteristic and buoy motions under Mathieu instability, for simplicity, the heave and pitch motion are expressed with considering the harmonic wave exciting. The natural frequency of heave and pitch motion are calculated in theory, which can prove the experiment design reference. In order to explain the occurring of large motion of the buoy in theory, the Mathieu equation of the pitch motion was expressed and the stability of the Mathieu equation was plotted.

2.2 Buoy motion regular wave

In this section, buoy motions are expressed by equations. And the parametric pitch resonance oscillation is also discussed from the viewpoint of the Mathieu-type instability. As shown in Figure 2.1, the wave direction is defined to be X-axis positive direction. The vertical displacement of buoy is defined by $z(t)$. And the positive Z-axis is vertical down. The buoy fluctuating with wave level (effective wave slope) is assumed, and the incident wave height is

$$h(t) = h_0 \sin(\omega t - kx) \tag{2.1}$$

where

h_0 : amplitude of the incident wave

ω : wave angular frequency

k : wave number and equals to ω^2/g

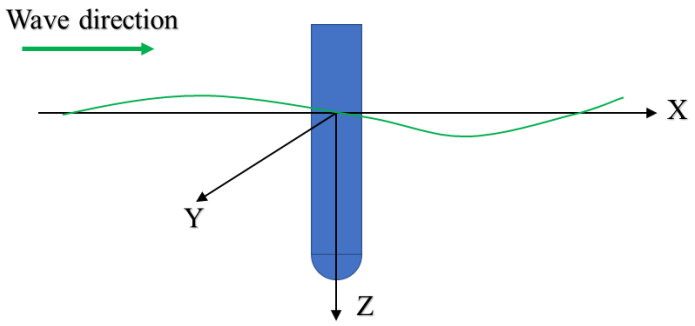

Figure 2.1 Coordinate diagram of the buoy and wave direction.

For simplicity, wave exciting force is treated as a single harmonic. Base on Newton's second law, the linear differential equation of heave motion can be expressed as follows:

$$m\ddot{z}(t) + R\dot{z}(t) + Sz(t) = F(t) \tag{2.2}$$

Wave exciting force is

$$F(t) = F_a \sin(\omega t + \varphi_F) \tag{2.3}$$

where φ_F is phase constant f and F_a is amplitude for the exciting force

Divide Equation (2.2) by *m*, the equation becomes

$$\ddot{z}(t) + 2\delta\dot{z}(t) + \omega_{nz}^2 z(t) = \frac{F(t)}{m} \tag{2.4}$$

When considering non-exciting force $F(t) = 0$, the Equation (2.4) becomes

$$\ddot{z}(t) + 2\delta\dot{z}(t) + \omega_{nz}^2 z(t) = 0 \tag{2.5}$$

where

the damping coefficient $\delta = R/2m$

the undamped nature angular frequency $\omega_{\mathrm{nz}} = \sqrt{S/m}$

the damped angular frequency $\omega_{nd} = \sqrt{{\omega_{nz}}^2 - \delta^2}$

The particular solution of Equation (2.4) is expressed by

$$\mathrm{z}^*(t) = Z_a \sin(\omega t + \varphi_z) \tag{2.6}$$

where φ_z is phase constant for the heave displacement is and Z_a is the excursion amplitude.

The heave velocity $u(t)$ and acceleration *a(t)* is obtained as follows:

$$u(t) = \dot{z}^*(\mathrm{t}) = \omega Z_a \cos(\omega t + \varphi_z) \tag{2.7}$$

$$a(t) = \ddot{z}^*(\mathrm{t}) = -Z_a \omega^2 \sin(\omega t + \varphi_z) \tag{2.8}$$

Insert the Equation (2.7) and (2.8) into Equation (2.4), Equation (2.4) becomes

$$Z_a\sqrt{(\omega^2 - \omega_{nh}^2)^2 + (4\delta\omega)^2}\cos(\omega t + \varphi_z + \varphi) = F_{\mathrm{a}} \sin(\omega t + \varphi_F) \tag{2.9}$$

Where phase constant for the heave velocity is

$$\varphi = \varphi_F - \varphi_z = \tan^{-1}\left(\frac{2\delta\omega}{\omega^2 - \omega_{nh}^2}\right) \tag{2.10}$$

$$Z_a = \frac{F_{\mathrm{a}}}{\omega\sqrt{(S/\omega - m\omega)^2 + R^2}} \tag{2.11}$$

Set $\Lambda_h = \frac{\omega}{\omega_{nh}}$ is frequency ratio of heave motion, which is called as tuning factor of heave motion.

And the phase difference between exciting force and heave velocity is

$$\varphi_h = \varphi_F - \varphi_u = \tan^{-1}\left(\frac{{\Lambda_h}^2 - 1}{2\nu\Lambda_h}\right) \tag{2.12}$$

where $\nu = \frac{\delta}{\omega_{nh}}$ is damping factor.

The Equation (2.11) is rewritten by

$$Z_a = \frac{F_a}{S}\frac{1}{\sqrt{(1-\Lambda_h)^2+(2\nu\Lambda_h)^2}} \tag{2.13}$$

Based on Equation (2.13), the diagram of phase-frequency response of heave motion is plotted, as shown in Figure 2.2.

The static excursion under the dynamic load with the amplitude F_0 is defined by $Z_{st} = \frac{F_a}{S}$.

ξ is the nondimensionalized excursion ratio and called by dynamical magnification factor of heave motion, which means the ratio of Z_a to Z_{st}. Equation (2.13) becomes

$$\xi = \frac{Z_a}{Z_{st}} = \frac{1}{\sqrt{\left(1-\Lambda_h^2\right)^2+(2\nu\Lambda_h)^2}} \tag{2.14}$$

Based on Equation (2.14), amplitude-frequency response of heave motion is plotted in Figure 2.3. For the different ratio ν, the corresponding oscillation curves are different. By means of varying the value of Λ_h, the oscillation response of the system can be controlled to some extent.

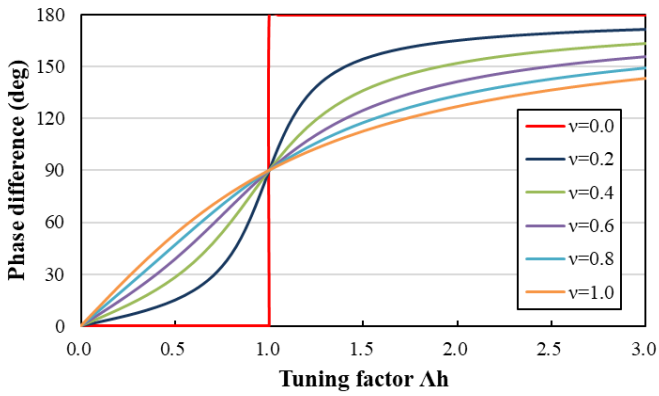

Figure 2.2 Phase-frequency response of heave motion.

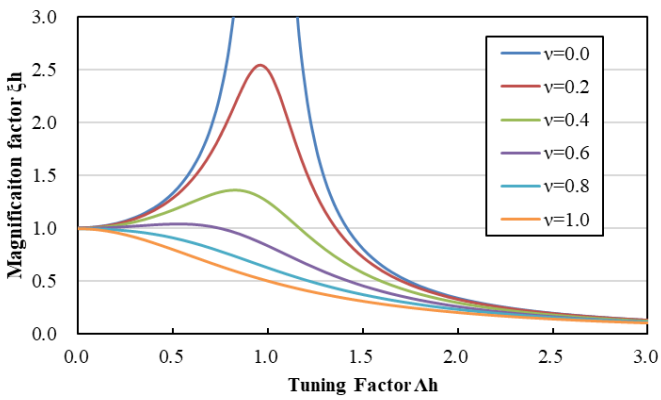

Figure 2.3 Amplitude-frequency response of heave motion.

For simplicity, the pitch motion is considered as a single harmonic oscillation without wave exciting moment and express the pitch angle by φ. According to the principle of dynamic equilibrium, the total moment $\sum M = 0$, the equation of pitch motion can be expressed as follows:

$$M(\ddot{\varphi}) + M(\dot{\varphi}) + M(\varphi) + M_{wave} = 0$$

$$(I + I')\ddot{\varphi}(t) + N_{\varphi}\dot{\varphi} + \Delta\overline{GM}\varphi(t) - \Delta\overline{GM}kh_0 \cos\omega t = 0 \qquad (2.15)$$

Where

I —— the inertia moment of the buoy

I' —— the added inertia moment

N_{φ} —— the damping coefficient

$\overline{GM}$ —— the metacentric height

Δ —— the displacement

Divided both sides of Equation (2.15) by inertia moment $I + I'$, the equation can be rewritten as follows:

$$\ddot{\varphi}(t) + 2\nu_{\varphi}\omega_n\dot{\varphi}(t) + \omega_n^2\varphi(t) - \omega_{np}^2 kh_0 \cos\omega t = 0 \qquad (2.16)$$

where

ω_n —— the natural frequency of pitch motion $\quad \omega_{np} = \sqrt{\frac{\Delta\overline{GM}}{I+I'}}$

ν_{φ} —— the damping ratio $\quad \nu_{\varphi} = \frac{N_{\varphi}}{2\sqrt{\Delta\overline{GM}(I+I')}}$

The particular solution of Equation (2.16) is assumed as follows:

$$\varphi^*(t) = \varphi_a \, sin(\omega t - \varepsilon_{\varphi}) \qquad (2.17)$$

where ε_{φ} is constant phase for the pitch motion.

The differential and second differential of Equation (2.17) are

$$\dot{\varphi} = \omega\varphi_a \, cos(\omega t - \varepsilon_{\varphi}) \qquad (2.18)$$

$$\ddot{\varphi} = -\omega^2\varphi_a \, sin(\omega t - \varepsilon_{\varphi}) \qquad (2.19)$$

Substituting the Equation (2.17) (2.18) and (2.19) into the Equation (2.16), Equation (2.16) becomes

$$-\omega^2\varphi_a \, sin(\omega t - \varepsilon_{\varphi}) + 2\nu_{\varphi}\omega_{np}\omega\varphi_a \, cos(\omega t - \varepsilon_{\varphi}) + \omega_{np}^2\varphi_a \, sin(\omega t - \varepsilon_{\varphi}) - \omega_{np}^2 kh_0 \cos\omega t = 0$$

$$\begin{aligned} -\omega^2\varphi_a \, sin\,\omega t \cos\varepsilon_{\varphi} + \omega^2\varphi_a \cos\omega t \sin\varepsilon_{\varphi} + 2\nu_{\varphi}\omega_n\omega\varphi_a \cos\omega t \cos\varepsilon_{\varphi} \\ + 2\nu_{\varphi}\omega_{np}\omega\varphi_a \sin\omega t \sin\varepsilon_{\varphi} + \omega_{np}^2\varphi_a \, sin\,\omega t \cos\varepsilon_{\varphi} - \omega_{np}^2\varphi_a \cos\omega t \sin\varepsilon_{\varphi} \\ - \omega_{np}^2 kh_0 \cos\omega t = 0 \end{aligned} \qquad (2.20)$$

Dividing in the sin and cosine terms, the following equation is obtained

$$\begin{aligned} \left[-\omega^2\varphi_a \cos\varepsilon_{\varphi} + 2\nu_{\varphi}\omega_{np}\omega\varphi_a \sin\varepsilon_{\varphi} + \omega_{np}^2\varphi_a \cos\varepsilon_{\varphi}\right] sin(\omega t) + \\ \left[\omega^2\varphi_a \sin\varepsilon_{\varphi} + 2\nu_{\varphi}\omega_{np}\omega\varphi_a \cos\varepsilon_{\varphi} - \omega_{np}^2\varphi_a \sin\varepsilon_{\varphi} - \omega_{np}^2 kh_0\right] cos(\omega t) = 0 \end{aligned} \qquad (2.21)$$

The coefficient of the sine and cosine term should be zero, the equation becomes

$$-\omega^2\varphi_a\cos\varepsilon_\varphi + 2\nu_\varphi\omega_n\omega\varphi_a\sin\varepsilon_\varphi + \omega_n^2\varphi_a\cos\varepsilon_\varphi = 0 \tag{2.22}$$

$$\omega^2\varphi_a\sin\varepsilon_\varphi + 2\nu_\varphi\omega_n\omega\varphi_a\cos\varepsilon_\varphi - \omega_n^2\varphi_a\sin\varepsilon_\varphi + \omega_n^2 kh_0 = 0 \tag{2.23}$$

Solve the Equation (2.23), ε_φ can be obtained as follows:

$$\tan\varepsilon_\varphi = \frac{\omega^2-\omega_{np}^2}{2\nu_\varphi\omega_{np}\omega} \tag{2.24}$$

$$\sin\varepsilon_\varphi = \frac{\omega^2-\omega_{np}^2}{\sqrt{\left(\omega^2-\omega_{np}^2\right)^2+4\nu_\varphi^2\omega_{np}^2\omega^2}} \tag{2.25}$$

$$\cos\varepsilon_\varphi = \frac{2\nu_\varphi\omega_{np}\omega}{\sqrt{\left(\omega^2-\omega_{np}^2\right)^2+4\nu_\varphi^2\omega_{np}^2\omega^2}} \tag{2.26}$$

From Equation (2.24), the phase difference between exciting force and pitch angle velocity is $\varphi_p = \varepsilon_\varphi$ and is solved as follows:

$$\varphi_p = \tan^{-1}\left(\frac{\omega^2-\omega_{np}^2}{2\nu_\varphi\omega_{np}\omega}\right) = \tan^{-1}\left(\frac{\Lambda_p^2-1}{2\nu_\varphi\Lambda_p}\right) \tag{2.27}$$

where $\Lambda_p = \frac{\omega}{\omega_{np}}$ is frequency ratio between frequency of exciting force and natural frequency of pitch motion, which is also called as tuning factor for pitch motion.

The phase difference of excited force and pitch angular velocity $\varphi_p{}'$ is shown as follows:

$$\varphi_p{}' = \varphi_p + \frac{\pi}{2} = \tan^{-1}\left(\frac{1-\Lambda_p^2}{2\nu_\varphi}\right) + \frac{\pi}{2} \tag{2.28}$$

Based on Equation (2.28), the phase-frequency response of pitch motion is plotted in Figure 2.4.

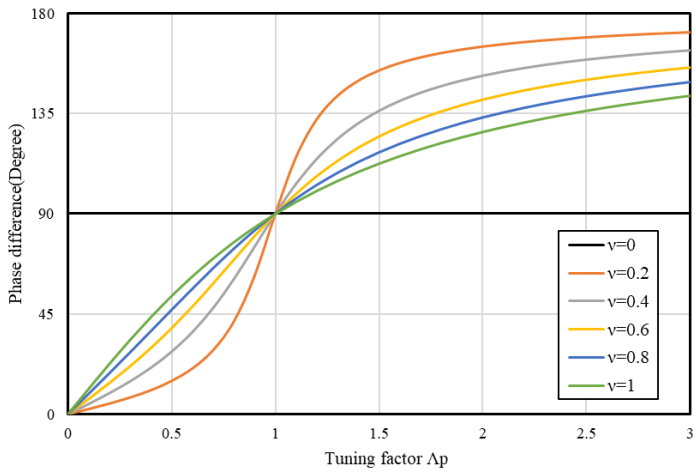

Figure 2.4 Phase-frequency response of pitch motion.

Substitute the Equation (2.25) and Equation (2.26) into Equation (2.23), the equation becomes

$$\left[\frac{\omega^4+4\nu_\varphi^2\omega_{np}^2\omega^2+\omega_{np}^4-2\omega_{np}^2\omega^2}{\sqrt{\left(\omega^2-\omega_{np}^2\right)^2+4\nu_\varphi^2\omega_{np}^2\omega^2}}\right]\varphi_a=\omega_{np}^2kh_0 \tag{2.29}$$

$\xi_p=\frac{\varphi_a}{kh_0}$ is the nondimensionalized excursion ratio and called by dynamical magnification factor of pitch motion, Equation (2.29) becomes

$$\xi_p=\frac{\varphi_a}{kh_0}=\frac{\omega_{np}^2\sqrt{\left(\omega^2-\omega_{np}^2\right)^2+4\nu_\varphi^2\omega_{np}^2\omega^2}}{\omega^4+4\nu_\varphi^2\omega_{np}^2\omega^2+\omega_{np}^4-2\omega_{np}^2\omega^2}=\frac{\omega_{np}^2}{\sqrt{\left(\omega^2-\omega_{np}^2\right)^2+4\nu_\varphi^2\omega_{np}^2\omega^2}}=\frac{1}{\sqrt{\left(\Lambda_p^2-1\right)^2+4\nu_\varphi^2\Lambda_p^2}} \tag{2.30}$$

Based on Equation (2.30), the amplitude-frequency response of pitch motion is plotted in Figure 2.5.

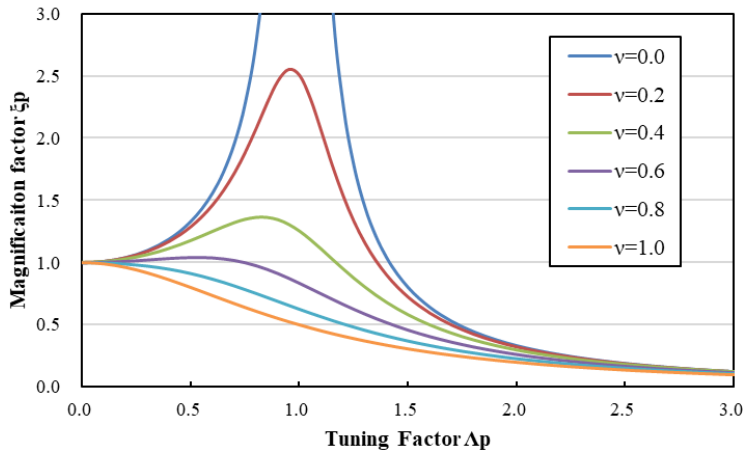

Figure 2.5 Amplitude-frequency response of pitch motion.

2.3 Mathieu equation

The resonant condition of heave oscillation of a buoy is assumed. The vertical displacement of the buoy can be expressed as follows:

$$z(t)=\frac{h_0}{2\nu_z}\sin\left(\omega_{nh}t-\frac{\pi}{2}\right),\quad \omega_{nh}=\sqrt{\frac{\rho g A_W}{m+m'}} \tag{2.31}$$

where,

ρ : density of water

g : gravitational acceleration

A_w : water plane area of the buoy

$m+m'$: virtual mass of the buoy

Then the relative water level is defined as follows:

$$\zeta(t) = z(t) - h(t) = -\zeta_0 \, sin\left(\omega_{nh} t + \varepsilon_\zeta\right) \tag{2.32}$$

where

$$\zeta_0 = \frac{h_0}{2\nu_{nh}}\sqrt{1 + 4\nu_z^2}, \quad \varepsilon_\zeta = tan^{-1}\left(\frac{1}{2\nu_{nh}}\right) \tag{2.33}$$

In Equation (2.16), according to the relative water level, the $\Delta\overline{GM}$ becomes functions of time and can be written as follows:

$$\Delta(t) = \Delta_0 + \rho g A_W \zeta(t) \tag{2.34}$$

$$\overline{GM}(t) = \overline{BM}(t) - \overline{OB}(t) + \overline{OG}(t) \tag{2.35}$$

$$\Delta(t)\overline{GM}(t) \cong \Delta_0 \overline{GM_0}\left\{1 - S_\phi \sin\left(\omega_{nh} t + \varepsilon_\zeta\right)\right\} \tag{2.36}$$

where

$$S_\phi = \frac{\rho g A_W \zeta_0 \overline{OG_0}}{\Delta_0 \overline{GM}_0} \tag{2.37}$$

$\overline{OG}_0, \Delta_0$ and $\overline{GM}_0$ show the centre of gravity, the displacement and the metacentric height in still water.

Substitute Equation (2.36) into Equation (2.16) and divided both sides by $I + I'$, the equation of motion can be rewritten as follows:

$$\ddot{\varphi}(t) + 2\nu_\varphi \omega_{np} \dot{\varphi}(t) + \omega_{\phi n}^2\left\{1 - S_\phi \sin\left(\omega_{nh} t + \varepsilon_\zeta\right)\right\}\varphi = 0 \tag{2.38}$$

where the pitch natural frequency ω_{pn} and the damping ratio ν_φ are expressed as follows.

$$\omega_{np} = \sqrt{\frac{\Delta_0 \overline{GM_0}}{I + I'}}, \quad \nu_\varphi = \frac{N_\phi}{2\sqrt{\Delta_0 \overline{GM_0}(I + I')}} \tag{2.39}$$

Here, a new variable is introduced to remove the damping component and transform Equation (2.38) into the Mathieu equation.

$$\varphi(t) = \phi(t) \cdot e^{-\nu_\varphi \omega_{np} t} \tag{2.40}$$

Substitute Equation (2.40) for ϕ in Equation (2.38), the Mathieu equation can be obtained as follows:

$$\ddot{\phi}(t) + \left\{\omega_n^2 - a \sin\left(\omega_{nh} t + \varepsilon_\zeta\right)\right\}\phi(t) = 0 \tag{2.41}$$

where

$$\omega_n^2 = \omega_{np}^2\left(1 - \nu_\varphi^2\right) \tag{2.42}$$

$$a = \frac{S_\phi \omega_n^2}{1-\nu_\varphi^2} \tag{2.43}$$

As is well known, the fluctuating restoring moment term, which is expressed by the sine function in Equation (2.41), is the source of the instability (hereafter called "fluctuating coefficient"). The solution becomes unstable when $\omega_{nh} = 2\omega_n$ and can be approximated by the following form.

$$\phi(t) = -Ce^{\frac{a}{2\omega_{nh}}t} sin\left(\frac{\omega_{nh}}{2}t + \frac{\varepsilon_\zeta}{2}\right) \tag{2.44}$$

$$\varphi(t) = -Ce^{\left(\frac{a}{2\omega_{nh}} - \nu_\varphi \omega_{np}\right)t} sin\left(\frac{\omega_{nh}}{2}t + \frac{\varepsilon_\zeta}{2}\right) \tag{2.45}$$

where C is a positive constant to be determined by the initial conditions.
Therefore, if the condition expressed by

$$\frac{a}{2\omega_{nh}} > \nu_\varphi \omega_{np} \tag{2.46}$$

is satisfied, the pitch amplitude becomes larger and larger as time proceeds.

Figure 2.6 shows the phase relationship among the heave motion expressed by Equations (2.31), the fluctuating coefficient of Equation (2.41) and the pitch angle expressed by Equation (2.44) to observe the actual timing of each signal under the Mathieu-type instability. For simplicity, amplitudes of the signals are indicated by unit amplitudes in the graph. Looking at the phase relationship between the pitch motion (blue line) and the fluctuating coefficient (green line), it can be observed that the fluctuating coefficient takes positive value during the pitch motion is returning to the equilibrium position. On the contrary, the fluctuating coefficient takes negative value when the pitch motion is leaving to the equilibrium position. That is the physical explanation of the Mathieu-type instability. On the other hand, looking at the relationship between the pitch angle (blue curve) and the heave acceleration (red curve), it can be observed that the heave acceleration takes negative value during the pitch motion is returning to the equilibrium position. This can be understood easily because negative value of the relative water level, which is defined by Equation (2.32), can reduce the pitch stability as shown by Equation (2.36).

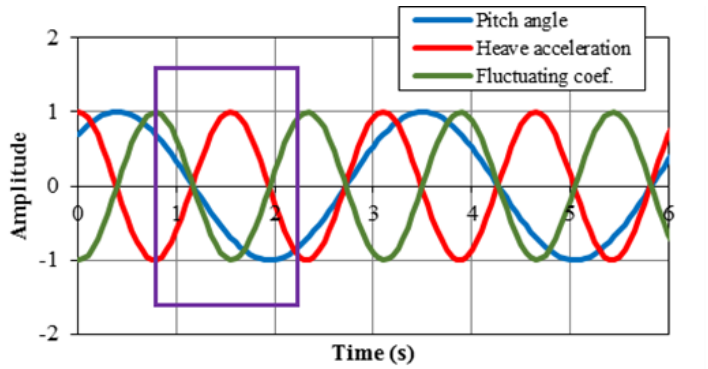

Figure 2.6 The history of coefficient of the pitch motion, heave acceleration and the restoring force coefficient.

2.4 Mathieu stability chart

A new variable is introduced to remove the damping component

$$\ddot{\phi}(\tau) + \{\delta + \varepsilon\, cos(\tau)\}\phi(t) = 0 \tag{2.47}$$

where

$$\delta = \frac{\omega_{np}^2}{\omega_{nh}^2}\left(1 - \nu_\phi^2\right),\ \varepsilon = \frac{\omega_{np}^2 S_\phi}{\omega_{nh}^2}, \tau = \omega_z t + \theta_\zeta + \frac{\pi}{2} \tag{2.48}$$

Based on the method of the Hill's infinite determinants [46, 47], the parametric curves about δ and ε can be obtained by four set of algebraic equation. Here, δ is called as the constant restoring coefficient and ε is called as the fluctuating restoring coefficient. It should be noted that τ in the Equation (2.49) was defined by Equation (2.50) and it is a new variable, which is different from the time *t*. The solution of the Equation (2.49) is given with the form of a Fourier series as follows.

$$\phi(t) = \sum_0^n \left\{a_n \cos\left(\frac{n\tau}{2}\right) + b_n \sin\left(\frac{n\tau}{2}\right)\right\} \tag{2.49}$$

Substitute Equation (2.49) into Equation (2.47) to calculate eigenvalues of the matrix, which is called as harmonic balance method. The sinusoidal and cosinoidal coefficients parts can be organized sinusoidal even part called as AA_{even}, sinusoidal odd part called as AA_{odd}, cosinoidal even part called as BB_{even} and cosinoidal odd part called as BB_{odd}, which are transferred by elementary and shown as follows:

$$\mathrm{AA_{even}} = \begin{bmatrix} 0 & \varepsilon/2 & 0 & 0 & & \\ \varepsilon & -1 & \varepsilon/2 & 0 & & \\ 0 & \varepsilon/2 & -4 & \varepsilon/2 & \cdots & \\ 0 & 0 & \varepsilon/2 & -9 & & \\ & & \vdots & & \ddots & \varepsilon/2 \\ & & & & \varepsilon/2 & -59^2 \end{bmatrix} \sim \begin{bmatrix} 0 & -\varepsilon/2 & 0 & 0 & & \\ -\varepsilon & 1 & -\varepsilon/2 & 0 & & \\ 0 & -\varepsilon/2 & 4 & -\varepsilon/2 & \cdots & \\ 0 & 0 & -\varepsilon/2 & 9 & & \\ & & \vdots & & \ddots & -\varepsilon/2 \\ & & & & -\varepsilon/2 & 59^2 \end{bmatrix}$$

$$\mathrm{BB_{even}}=\begin{bmatrix}-1 & \varepsilon/2 & 0 & 0 & & \\ \varepsilon/2 & -4 & \varepsilon/2 & 0 & & \\ 0 & \varepsilon/2 & -9 & \varepsilon/2 & \cdots & \\ 0 & 0 & \varepsilon/2 & -16 & & \\ & & \vdots & & \ddots & \varepsilon/2 \\ & & & & \varepsilon/2 & -30^2\end{bmatrix}\sim\begin{bmatrix}1 & -\varepsilon/2 & 0 & 0 & & \\ -\varepsilon/2 & 4 & -\varepsilon/2 & 0 & & \\ 0 & -\varepsilon/2 & 9 & -\varepsilon/2 & \cdots & \\ 0 & 0 & -\varepsilon/2 & 16 & & \\ & & \vdots & & \ddots & -\varepsilon/2 \\ & & & & -\varepsilon/2 & 30^2\end{bmatrix}$$

$$\mathrm{AA_{odd}}=\begin{bmatrix}-1/4+\varepsilon/2 & \varepsilon/2 & 0 & 0 & & \\ \varepsilon/2 & -9/4 & \varepsilon/2 & 0 & & \\ 0 & \varepsilon/2 & -25/4 & \varepsilon/2 & \cdots & \\ 0 & 0 & \varepsilon/2 & -49/4 & & \\ & & \vdots & & \ddots & \varepsilon/2 \\ & & & & \varepsilon/2 & -\frac{59^2}{4}\end{bmatrix}\sim\begin{bmatrix}\frac{1}{4}-\varepsilon/2 & -\varepsilon/2 & 0 & 0 & & \\ -\varepsilon/2 & 9/4 & -\varepsilon/2 & 0 & & \\ 0 & -\varepsilon/2 & 25/4 & -\varepsilon/2 & \cdots & \\ 0 & 0 & -\varepsilon/2 & 49/4 & & \\ & & \vdots & & \ddots & -\varepsilon/2 \\ & & & & -\varepsilon/2 & \frac{59^2}{4}\end{bmatrix}$$

$$\mathrm{BB_{odd}}=\begin{bmatrix}-\frac{1}{4}-\varepsilon/2 & \varepsilon/2 & 0 & 0 & & \\ \varepsilon/2 & -9/4 & \varepsilon/2 & 0 & & \\ 0 & \varepsilon/2 & -25/4 & \varepsilon/2 & \cdots & \\ 0 & 0 & \varepsilon/2 & -49/4 & & \\ & & \vdots & & \ddots & \varepsilon/2 \\ & & & & \varepsilon/2 & -\frac{59^2}{4}\end{bmatrix}\sim\begin{bmatrix}\frac{1}{4}+\varepsilon/2 & -\varepsilon/2 & 0 & 0 & & \\ -\varepsilon/2 & 9/4 & -\varepsilon/2 & 0 & & \\ 0 & -\varepsilon/2 & 25/4 & -\varepsilon/2 & \cdots & \\ 0 & 0 & -\varepsilon/2 & 49/4 & & \\ & & \vdots & & \ddots & -\varepsilon/2 \\ & & & & -\varepsilon/2 & \frac{59^2}{4}\end{bmatrix}$$

(2.50)

Equation (2.50) are rewritten by relative homogeneous linear equations, determinant matrix values of which are set to zero. The determinants are shown as follows:

$$a_{\mathrm{even}}:\begin{vmatrix}\delta & \varepsilon/2 & 0 & 0 & \\ \varepsilon & \delta-1 & \varepsilon/2 & 0 & \\ 0 & \varepsilon/2 & \delta-4 & \varepsilon/2 & \ldots \\ & & \vdots & & \end{vmatrix}=0 \tag{2.51}$$

$$b_{\mathrm{even}}:\begin{vmatrix}\delta-1 & 0 & 0 & 0 & \\ \varepsilon/2 & \delta-4 & \varepsilon/2 & 0 & \\ 0 & \varepsilon/2 & \delta-9 & \varepsilon/2 & \ldots \\ & & \vdots & & \end{vmatrix}=0 \tag{2.52}$$

$$a_{odd}:\begin{vmatrix}\delta-1/4+\varepsilon/2 & \varepsilon/2 & 0 & 0 & \\ \varepsilon/2 & \delta-9/4 & \varepsilon/2 & 0 & \\ 0 & \varepsilon/2 & \delta-25/4 & \varepsilon/2 & \ldots \\ & & \vdots & & \end{vmatrix}=0 \tag{2.53}$$

$$b_{odd}:\begin{vmatrix}\delta-\frac{1}{4}-\varepsilon/2 & \varepsilon/2 & 0 & 0 & \\ \varepsilon/2 & \delta-9/4 & \varepsilon/2 & 0 & \\ 0 & \varepsilon/2 & \delta-25/4 & \varepsilon/2 & \cdots \\ & & \vdots & & \end{vmatrix}=0 \tag{2.54}$$

Finally, the stable and unstable regions of the Mathieu equation (2.47) are determined. The above equations are tridiagonal matrix determinants. In order to increase the accuracy of calculation, the order of the determinants is valued by 30. For a given value ε, the corresponding value δ is

calculated by solving the eigenvalues of the determinants, computing of which was programmed by MATLAB. Figure 2.7 shows Mathieu stability chart. 'U' means the unstable region and 'S' means the stable region. When the the parameter of δ and ε is in "U" region, that is unstable region, the solution of Equation (2.47) is divergent. When the the parameter of δ and ε is in "S" region, that is stable region, the solution of Equation (2.47) is convergent. According to the parameter of δ and ε, the tendency of result or motions can be figured out directly. The method of analyzing Mathieu instability condition can be directly utilized to buoy motion, and results of stable or unstable motion be determined easily.

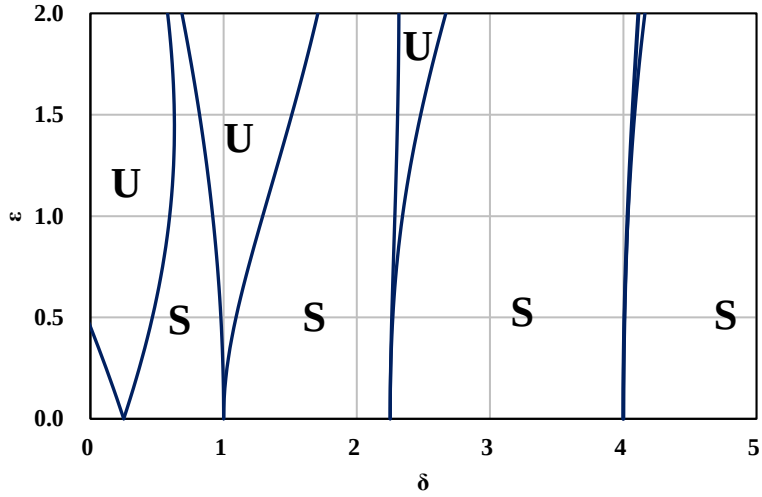

Figure 2.7 Mathieu stability chart.

2.5 Conclusion

The heave and pitch motion of the spar-type buoy are expressed with considering the harmonic wave exciting. The natural frequency of heave and pitch motion are calculated in theory, which can prove the experiment design reference and make the characteristic of the buoy satisfy the Mathieu instability condition (the natural frequency of the heave motion is twice of the pitch motion). The Mathieu equation of the pitch motion was expressed and occurring of large motion of the buoy was explained in theory. Moreover, the stability of the Mathieu equation was plotted, which can provide the theoretical reasons for the occurring of the large pitch in the later experiment.

Chapter3 Experiment work

3.1 Introduction

In order to investigate the coupled motion around the Mathieu-type instability condition, the corresponding experiment should be carried out. When the natural frequency of heave and the pitch motion satisfy Mathieu instability condition, the large motion will occur. In order to make the buoy satisfy this condition, the free-decay experiment is necessary is to be carried out. In this work, the ballast control system is designed to change the natural frequency of heave motion. Then the experiment in regular wave is carried out to verify the buoy motion characteristics under Mathieu instability condition.

3.2 Configuration of the spar-buoy

An innovative model is designed and made. The main body of cylindrical is made of transparent acrylic acid resin and a hemispherical aluminum ballast is attached to the bottom. The principal particulars of buoy model are listed in Table 3.1 and the appearance of the buoy model is shown in Figure 3.1. In order to investigate the coupled motion around the Mathieu-type instability condition, a ballast control mechanism was installed in the buoy model. The mechanism consists of weights, a step motor and a ball screw. The ball screw can shift the weights up and down so that the center of gravity of the buoy can be changed. Using this mechanism, the pitch natural frequency can be adjusted around half the heave natural frequency. The ballast position can be adjusted by the ball screw from 0 mm to 45 mm. The position is defined by the distance from the upper surface of the hemispherical ballast to the bottom surface of movable ballast. The specifications of buoy under different ballast positions are shown in Table 3.2.

Table 3.1 Principle particulars of the buoy model.

Item	Value
Depth	745 mm
Diameter of the buoy (Outer diameter)	160 mm
Weight	11.15 kg
Draught (from the bottom)	581.2 mm
Centre of buoyancy (from the bottom)	303.6 mm
Metacentric radius (BM)	2.89 mm
Ballast weight	2.74 kg
Ballast moving range	0~45 mm

In the experiments, the buoy model is likely to start swaying and yawing by the effect of the vortex induced vibration. Therefore, a flat metal bar was fixed on the top of the buoy model, and a restraining frame was also introduced and fixed on the carrier as shown in Figure 3.2. The actual condition of the experiments is shown in Figure 3.3.

Table 3.2 The specifications in the different ballast positions.

Ballast position (mm)	0	5	10	15	20	40
Centre of gravity (mm)	265.1	266.3	267.5	268.8	270.0	274.9
Inertia moment of pitch (kgm^2)	0.74	0.73	0.73	0.72	0.72	0.71
Metacentric height GM (mm)	41.4	40.2	39.0	37.7	36.5	31.6

Figure 3.1 Configuration of the spar-buoy model.

Figure 3.2 The restraining frame was fixed on the carrier.

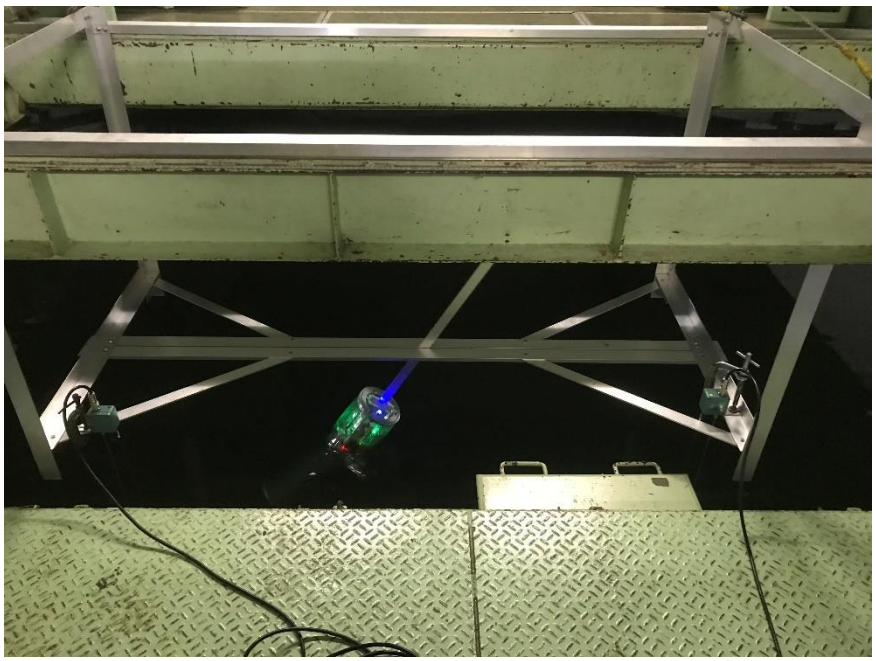

Figure 3.3 The restraining frame for sway, roll, yaw and lateral drift (surge, heave, pitch and longitudinal drift are free).

3.3 Control and measurement system

Figure 3.4 shows the ball screw mechanism driven by a step motor. The step motor driver is controlled by an Arduino Nano Mega328 and the control signals are received through the wireless transmission modules from the control PC which is shown in Figure 3.5. Nine axes accelerometer (Arduino 9 Axes Sensor Shield) is also installed in the buoy model to measure the buoy motions. The measured signals are also sent back through the wireless transmission modules to the control PC. The configuration of the measurement system is shown in Figure 3.6.

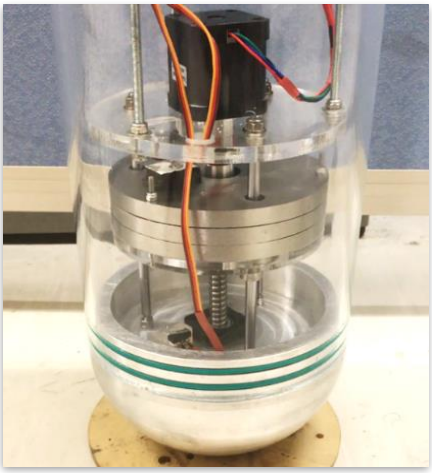

Figure 3.4 The ball screw mechanism driven by a step motor.

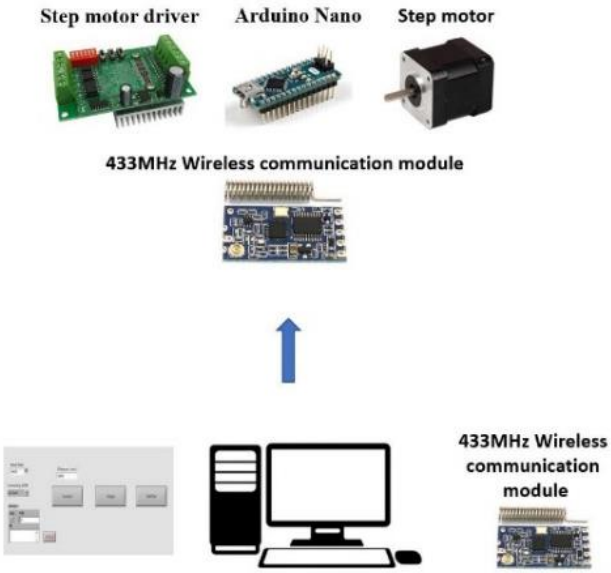

Figure 3.5 The ballast control system using wireless signal transmission module.

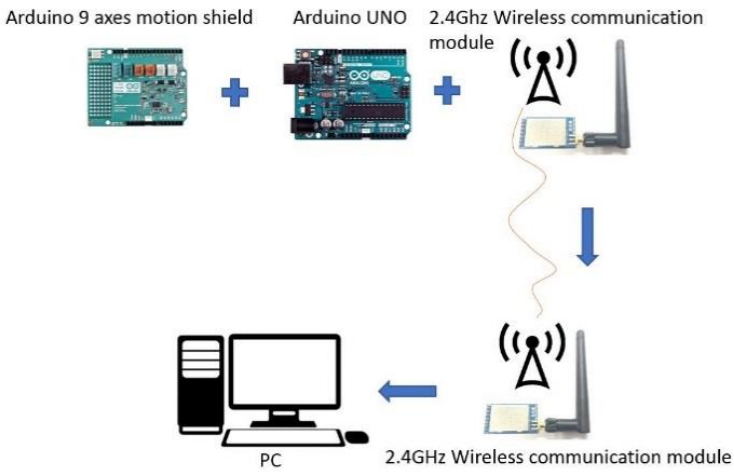

Figure 3.6 Wireless signal acquisition system for measurement of buoy motions.

3.4 Free-decay experiments

The experiments were conducted in the ship maneuvering research basin of TUMSAT. The principal dimensions and the photo are shown in Table 3.3 and Figure 3.7. The free-decay experiments were performed to determine the natural periods and damping coefficients of the heave and pitch motions.

Figure 3.7 Ship maneuvering research basin of TUMSAT.

Table 3.3 Principal dimensions of Ship maneuvering research basin of TUMSAT.

Length	54 m
Breadth	10 m
Depth	2 m
Wave maker	Flat plate type

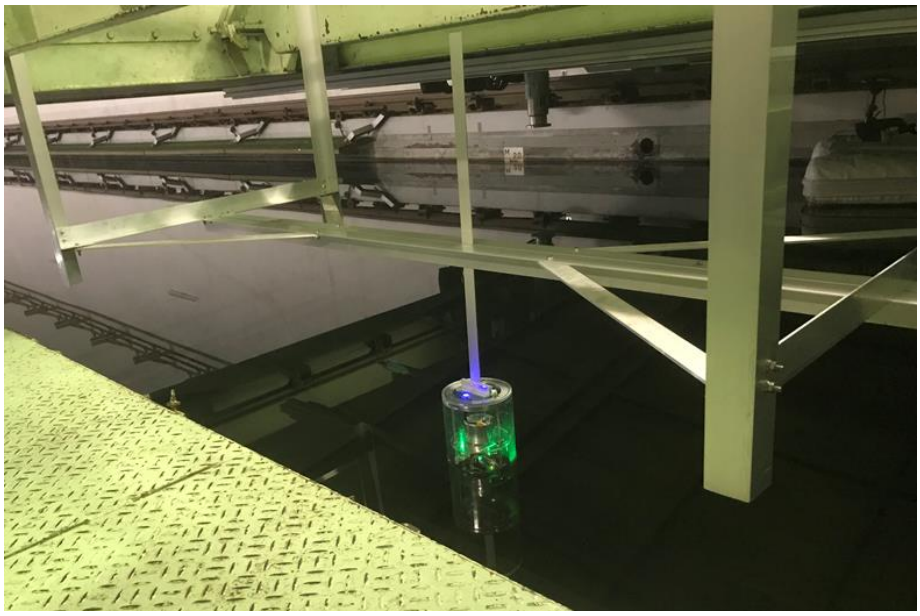

Figure 3.8 The free-decay experiment in still water.

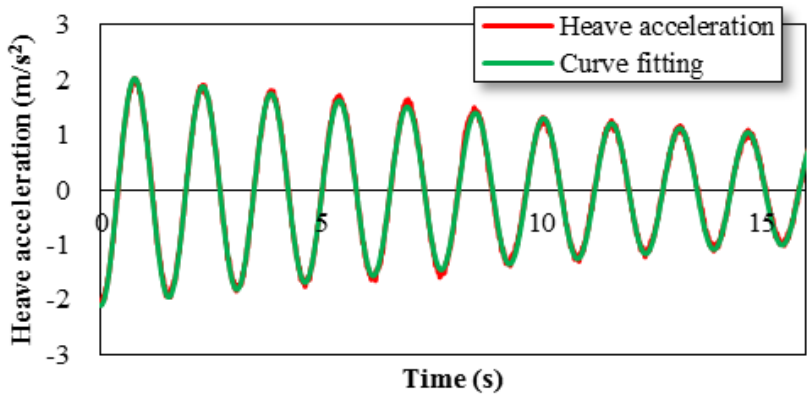

Figure 3.9 Measured time histories of heave acceleration (ballast position = 5 mm).

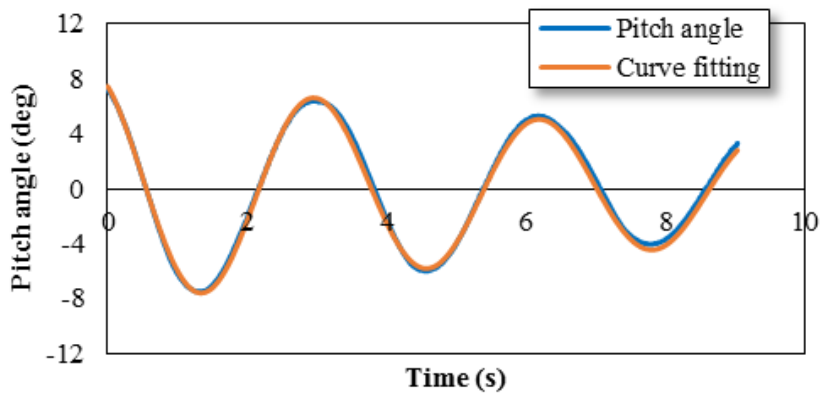

Figure 3.10 Measured time histories of pitch angle (ballast position = 5 mm).

The free-decay experiment was carried. Firstly, the buoy was put into the water as shown in Figure 3.8. Then the buoy was set at the initial small displacement in vertical direction and a small pitch angle separately by hand, and the free motions occurred. Figure 3.9 shows the heave acceleration measured by the accelerometer at the 5 mm ballast position. The signal was analyzed by fitting the following equation:

$$\ddot{z} = Ae^{\left(-\nu \pm i\sqrt{1-\nu^2}\right)\omega t} \tag{3.1}$$

where $\ddot{z}$ and A denote the heave acceleration and the amplitude, ν and ω are the damping ratio and the natural frequency.

The estimated natural period was 1.55s and the damping ratio was 0.013. Figure 3.10 shows the measured pitch angle at the 5mm ballast position. The signals of pitch motion were also analyzed by the similar curve fitting. The analyzed pitch natural periods at the different ballast positions are listed in Table 4 and the damping ratio was 0.038. As shown in Table 3.4, it can be found that the 5mm ballast position is closest to the Mathieu-type instability condition (the heave natural period is almost half of the pitch natural period).

Table 3.4 The pitch natural frequency at the different ballast positions.

Ballast position	Period
0 mm	2.93 s
5 mm	3.24 s
15 mm	3.26 s
20 mm	3.30 s

3.5 The experiment in regular waves

The motions of the buoy was measured with regular waves. The period of the incident waves was set to the heave natural period (1.55s) and waves height was 0.040m, as shown in Figure 3.11. In order to decrease the error, two waves height meters called “A” and “B” were installed to measure the actual waves height and period before carrying out the experiment. The waves height meters were put into the acrylic sink, as shown in Figure 3.12. The date of signal voltage with different water heights were measured to calculate the piezo voltage coefficient.

Figure 3.11 The PC control interface of waves maker.

Figure 3.12 The PC control interface of waves maker.

Figure 3.12 shown the measured result. The calculated coefficients of the waves height meter “A” and “B” are 0.1247 v/cm and 0.1244 v/cm.

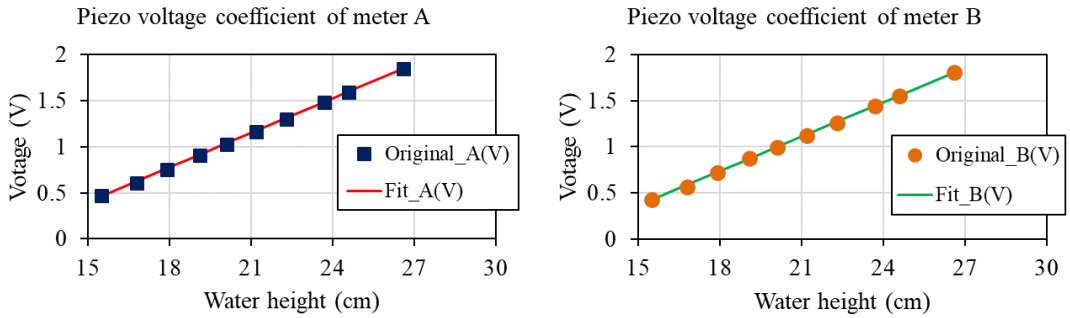

Figure 3.12 The measured piezo voltage results with different water heights.

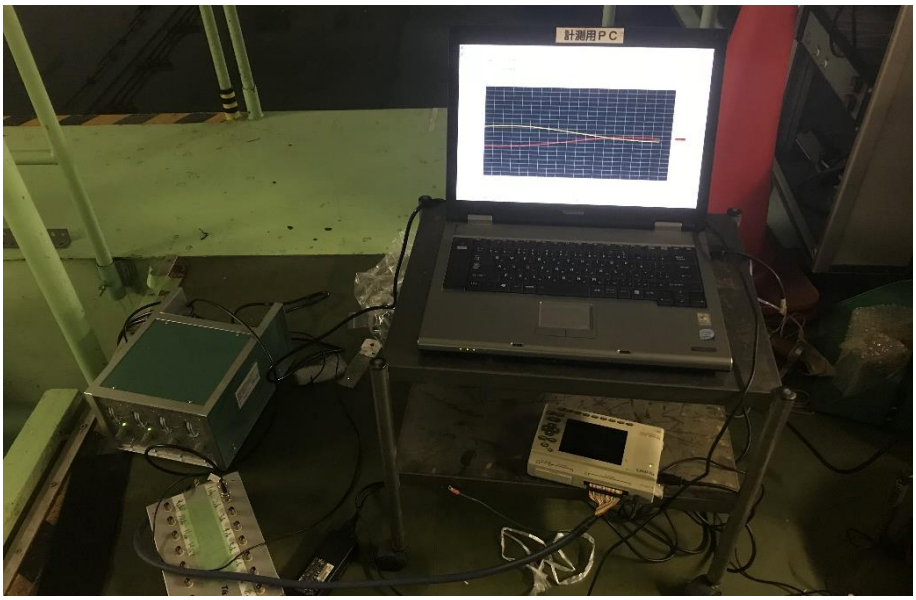

Figure 3.13 The PC control interface of waves maker.

Figure 3.13 shows the signal acquisition interface of two wave height meters. The results are shown in Figure 3.14 and Figure 3.15. And the “Date1” and “Data2” are the singal date of waves height “A” and “B”. The test results accord with the data curves of Least Squares, and the test proves the feasibility. The actual waves height and period were calculated and the both results are same. The actual period is 1.55s and the actual waves height is 0.042m.

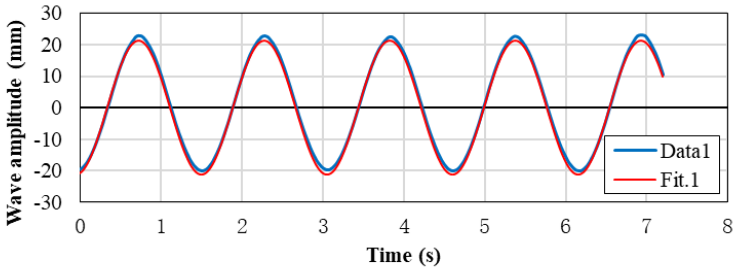

Figure 3.14 The actual waves wave height results of wave height meter "A".

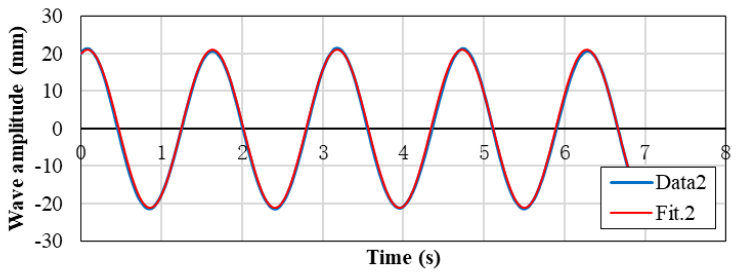

Figure 3.15 The actual waves wave height results of wave height meter "B".

After above experimental preparation, the motions of the buoy was measured with regular waves. Figure 3.16 a~f show the measured time histories of heave accelerations and pitch angles with ballast positions 0 ~ 40mm. Looking at the graphs, there are common characteristics as follows:

- The heave amplitude becomes larger alone in the first 10 seconds.
- Large pitch motions occur suddenly around 15 seconds.
- The heave amplitude shrinks just after the occurrence of large pitch motion.
- The kinetic energy of the large pitch motion seems to be supplied from the heave motion.

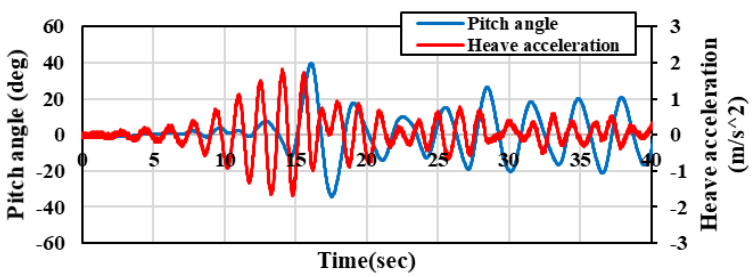

Figure 3.16a Measured time histories of pitch angle and heave acceleration (ballast position = 0 mm).

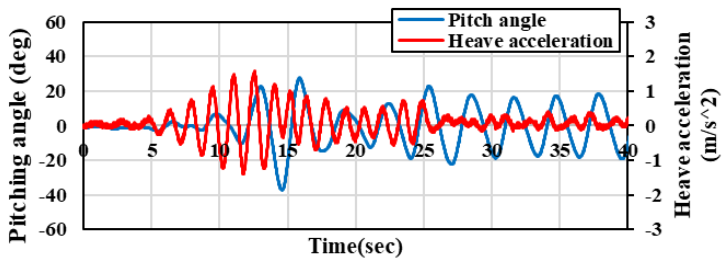

Figure 3.16b Measured time histories of pitch angle and heave acceleration (ballast position = 5 mm).

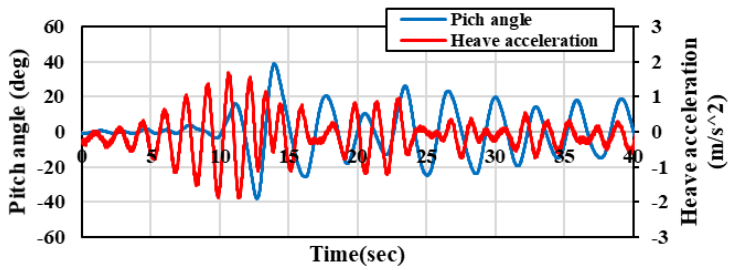

Figure 3.16c Measured time histories of pitch angle and heave acceleration (ballast position = 10 mm).

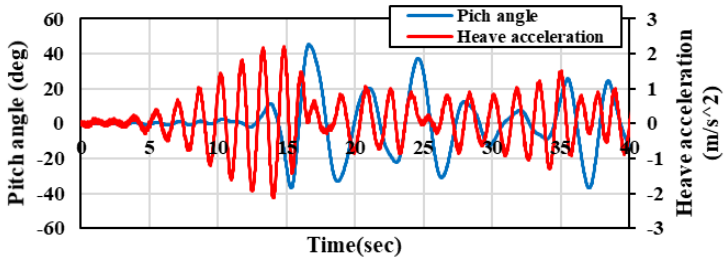

Figure 3.16d Measured time histories of pitch angle and heave acceleration (ballast position = 20 mm).

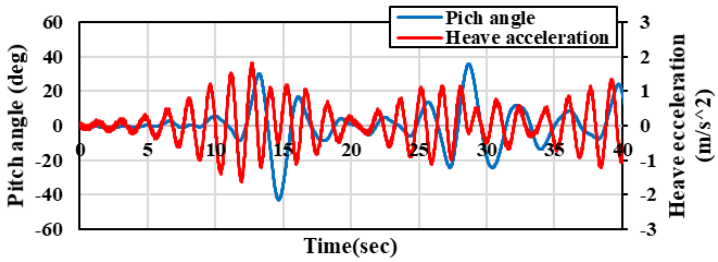

Figure 3.16e Measured time histories of pitch angle and heave acceleration (ballast position = 30 mm).

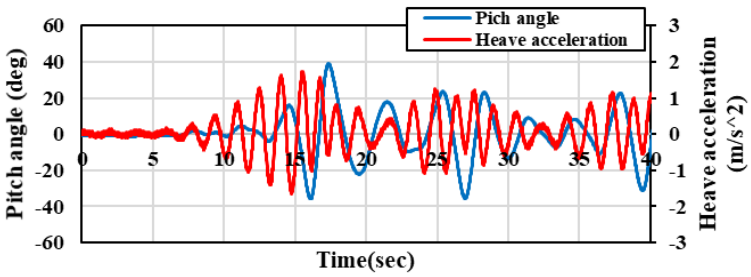

Figure 3.16f Measured time histories of pitch angle and heave acceleration (ballast position = 40 mm).

3.6 Wave-induced force

In order to investigate the wave force on the buoy, the wave-induced force experiment was carried out in towing tank with the buoy fixed on carrier. As shown in Figure 3.17, the coefficients of three-component force gauge were measured in preparation. The measured result is shown in Figure 3.18. “Fx” is the fore in x-axis (wave coming direction), “Fz” is the force in vertical direction and “My” is the moment is trim angle axis. The corresponding coefficients are -1.919 kg/V, 1.905 kg/V and 4.695 kg*m/V.

Figure 3.17 The coefficients of three-component force gauge were measured.

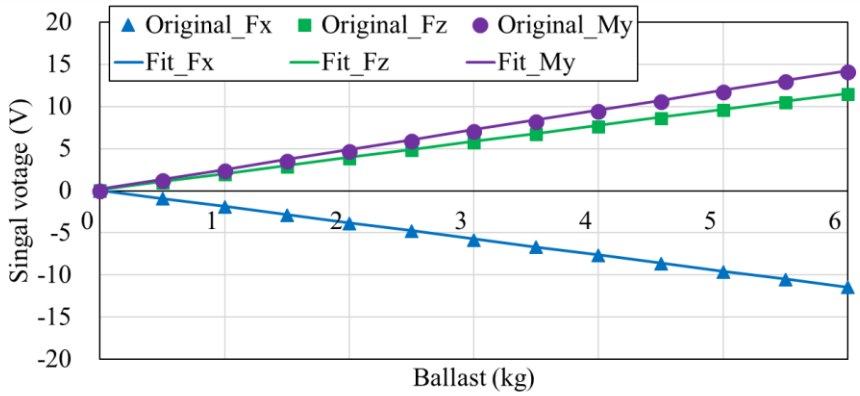

Figure 3.18 The result of measured three-component force gauge coefficients.

The fixed structure in Figure 3.19 is installed to test the wave exciting force with different trim angle. It can also be found there are two wave height meters to installed assure the accuracy of the experiment. The fix device can rotate the buoy with the different inclination (0 deg ~ 50deg), on the of which connected with three-component force gauge. The waterplane center of buoy and the wave height meters are on the same horizontal line which is perpendicular to wave coming direction. The data of acquisition will be recorded by amplifier and DAQ device as shown in Figure 3.20.

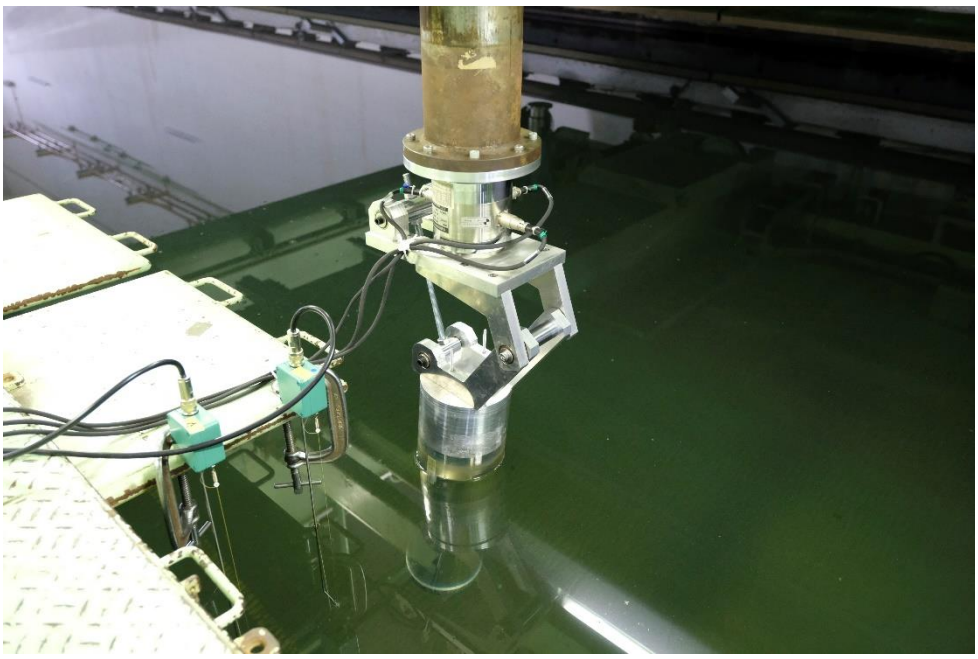

Figure 3.19 The wave-induced force testing.

In this experiment, the wave frequency is 1.55s, and the wave height is 4.2cm. The wave forces and wave heights were measured at the same, as shown in Figure 3.20. Figure 3.21 ~ Figure 3.24 show the wave-induced force results and the corresponding results of amplitudes are shown in Table 3.5. In this experiment, the trim angle is set by 0-degree, 5-degree, 10-degree and 20-degree. Here, *My* is pitch moment, Fz (N) is heave force and wave amplitude is the amplitude of the mad wave by wave maker.

Figure 3.20 Experimental data acquisition devices.

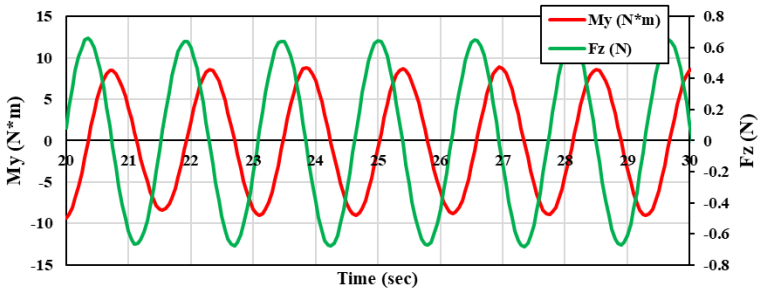

Figure 3.21 Wave-induced force with inclination angle 0 degree.

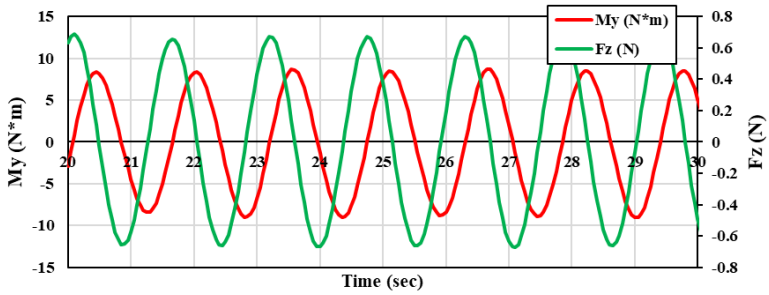

Figure 3.22 Wave-induced force with inclination angle 5 degree.

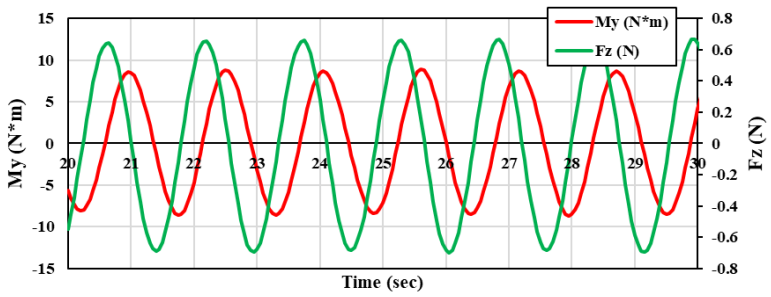

Figure 3.23 Wave-induced force with inclination angle 10 degree.

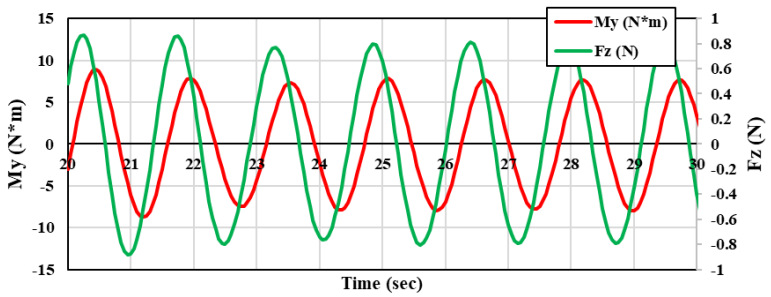

Figure 3.24 Wave-induced force with inclination angle 20 degree.

Table 3.5 The amplitude of the wave-induced force.

Trim angle (degree)	My (N*m)	Fz (N)	Wave amplitude (m)
0	8.752	0.661	0.024
5	8.624	0.670	0.024
10	8.561	0.678	0.024
20	7.783	0.802	0.023

3.7 Conclusion

The free-decay experiment was carried out to verify that the designed spar buoy can nearly satisfy the Mathieu instability condition (the natural frequency of heave motion is double the natural frequency of pitch motion). In order to investigate the coupled motion around the Mathieu-type instability condition in regular wave, the corresponding experiment was carried out with different ballast condition. It can be indicated that the large pitch motions occur suddenly around 15 seconds; the heave amplitude shrinks just after the occurrence of larger pitch motion and the kinetic energy of the large pitch motion seems to be supplied from the heave motion.

However, for the sake of completeness, this model still requires some improvements in future:

- The buoy oscillating motions were collected based on the acceleration gyroscope. With the changing of the ballast's position, the gravity center was also changed. The results of data acquisition keep error to some extent. To overcome this lack, the buoy will be designed to be able to be moved up and down, or a new acquisition data system, such as image acquisition, will be introduced. Moreover, there is resistance in the fixed frame. In order to achieve buoy oscillating much smoother, the limit of the slide rail system can be introduced.
- The length of the towing tank is 50m, and the experiment was carried out in middle of the towing tank. Due to the reflection of the made waves, the effective of data is just until about 40 seconds, after which the experiment results can't be referenced. If possible, the improved experiment carried out in the longer towing tank is necessary and meaningful.

Chapter4 Energy transfer analysis

4.1 Introduction

It is found that the kinetic energy of the large pitch motion seems to be supplied from the heave motion in the experiment results. Hence, in order to investigate existence of the energy transform, the signals of the heave acceleration were integrated with high pass filtering in the frequency domain and the vertical velocities and displacements of the buoy were calculated. Base on the integrated data and the original measured data, the kinetic and potential energy of heave and pitch motions were calculated. The energy transform of the buoy motions is discussed in time domain.

4.2 The calculation of the heave displacement

In order to investigate existence of the energy transfer, the kinetic and potential energy of heave and pitch motions is tried to be estimated from the measured signals. The signals of the heave acceleration were integrated with high pass filtering in the frequency domain and the vertical velocities and displacements of the buoy were calculated. The integral results were transformed to the time domain again to obtain the time history of the vertical displacements and the velocities. Figure 4.1a ~ 4.1e show the accelerations, velocities and displacements of the heave motion at the ballast position 0 ~ 40 mm. It can be recognized that the signals were integrated successfully.

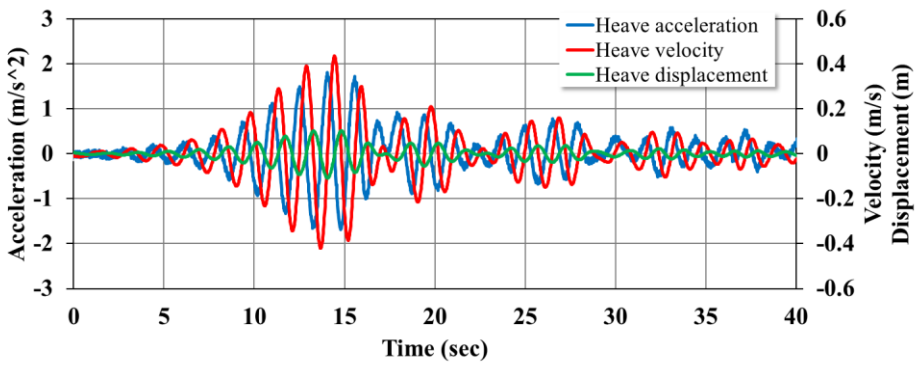

Figure 4.1a Acceleration, velocity and displacement of the heave motion (ballast position = 0 mm).

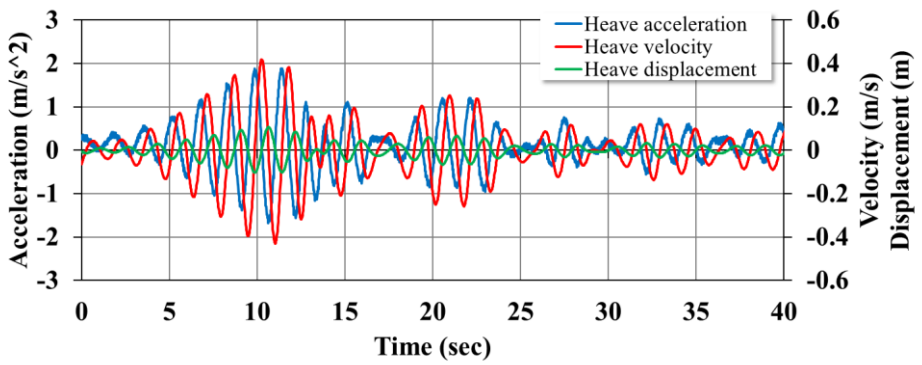

Figure 4.1b Acceleration, velocity and displacement of the heave motion (ballast position= 10 mm).

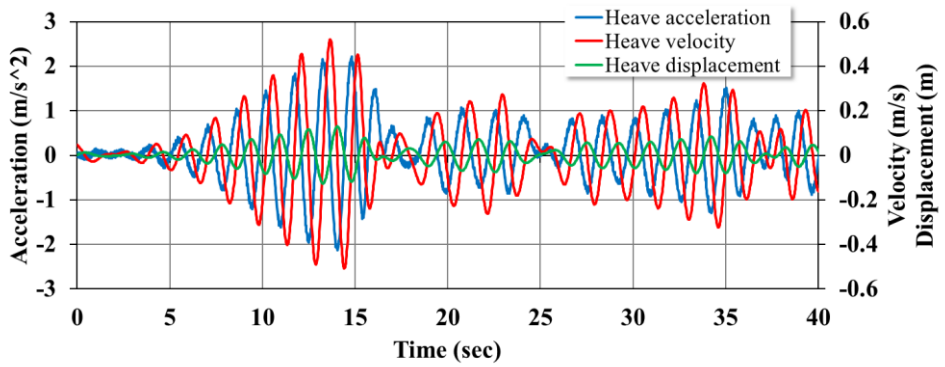

Figure 4.1c Acceleration, velocity and displacement of the heave motion (ballast position= 20 mm).

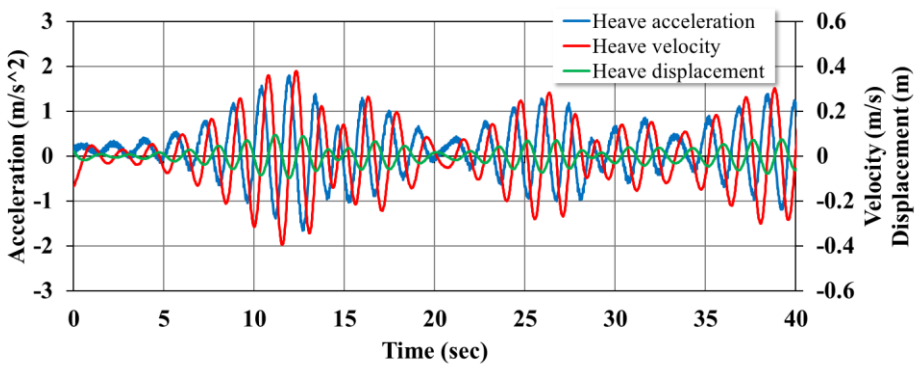

Figure 4.1d Acceleration, velocity and displacement of the heave motion (ballast position= 30 mm).

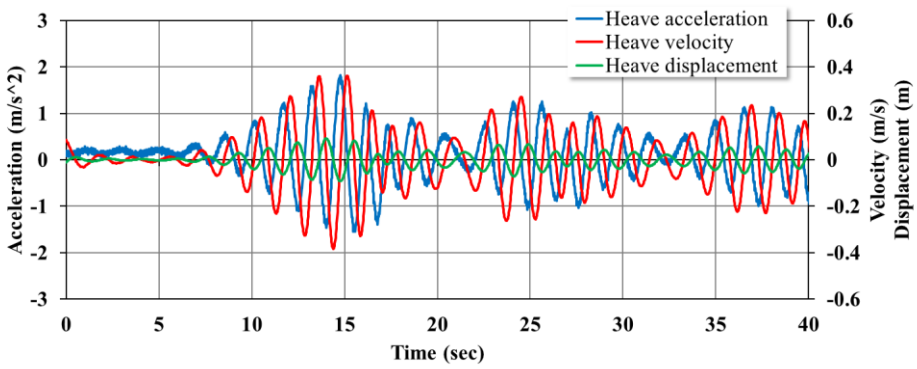

Figure 4.1e Acceleration, velocity and displacement of the heave motion (ballast position = 40 mm).

4.3 The analysis about the transformation of the kinetic energy

Using the integrated data and the original measured data, the kinetic and potential energy of heave and pitch motions were calculated. Figure 4.2a~4.2e show the time histories of the estimated energies at the ballast position 0 ~ 40 mm. The blue and red curves denote the energies of pitch and heave motions, respectively. Moreover, the green curves denote the total energy, namely, the sum of pitch and heave energy. Looking at the figures, the total energy takes the maximum value around 16s and the first half of the peak is dominated by the heave energy and the latter half is replaced by the pitch energy. Therefore, this can be concluded that the energy was transferred from the heave mode to the pitch mode and shrunken by the pitch damping. On the other hand, the power to be taken off is closely related to the total energy (area surrounded by the green curve and the horizontal axis). Therefore, the optimum ballast position can be determined from this point of view.

Figure 4.3 shows the zero crossing periods of the time histories in time history of heave motion, by the method of which, these periods in transient states of heave motion was measured. The the transition of the periods of pitch motion was also carried out by the same means.

Figure 4.4 shows the transition of the periods of pitch and heave motions. These periods in transient states were measured by the zero crossing periods of the time histories. The left and right vertical axes denote the pitch and heave periods, respectively. Here, it should be noted that the scale of the left vertical axis is twice with respect to the right. Therefore, the intersecting points of two lines mean that the Mathieu-type instability condition is satisfied. Looking at these figures, it can be observed that the first timing of the intersection coincides with the occurrence of the large pitch motion. Therefore, it may be able to find some conditions in which the large pitch motion occurs suddenly by considering the theoretical condition of the Mathieu-type instability.

Figure 4.5 and Figure 4.6 show the transition of the periods of pitch and heave motions. These periods in transient states were measured by the zero crossing periods of the time histories. The left and

right vertical axes denote the pitch and heave periods, respectively. Here, it should be noted that the scale of the left vertical axis is twice with respect to the right. Therefore, the intersecting points of two lines mean that the Mathieu-type instability condition is satisfied. Looking at these figures, it can be observed that the first timing of the intersection coincides with the occurrence of the large pitch motion. Therefore, it may be able to find some conditions in which the large pitch motion occurs suddenly by considering the theoretical condition of the Mathieu-type instability.

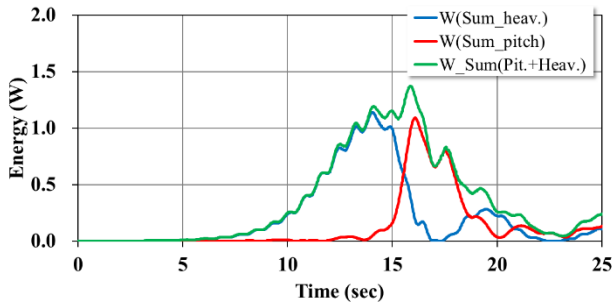

Figure 4.2a The energy time histories of the pitch angle and heave motion (ballast position = 0 mm).

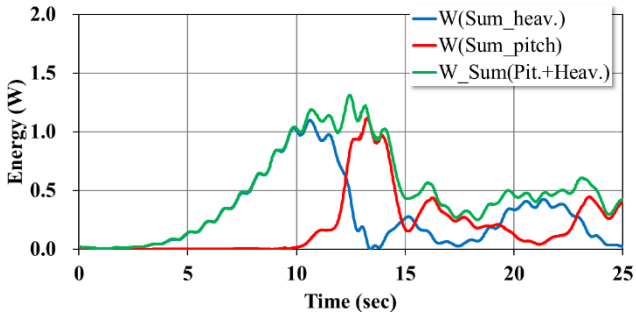

Figure 4.2b The energy time histories of the pitch angle and heave motion (ballast position = 10 mm).

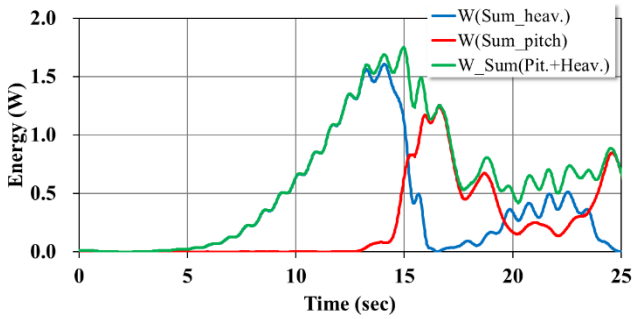

Figure 4.2c The energy time histories of the pitch angle and heave motion (ballast position = 20 mm).

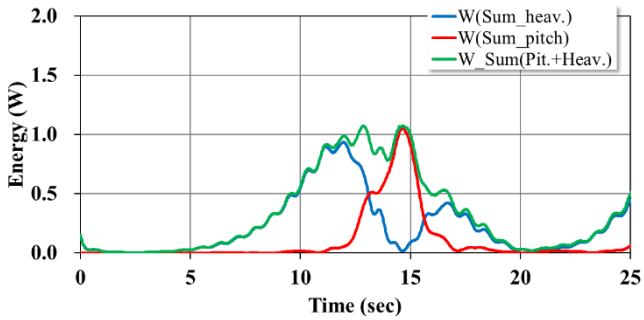

Figure 4.2d The energy time histories of the pitch angle and heave motion (ballast position = 30 mm).

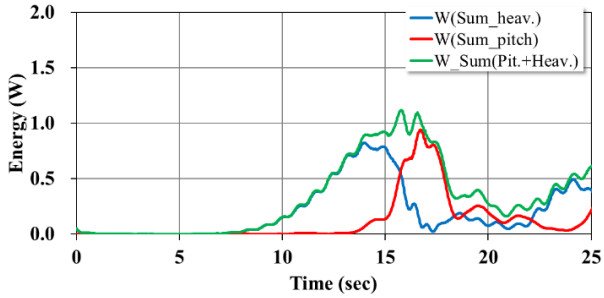

Figure 4.2e The energy time histories of the pitch angle and heave motion (ballast position = 40 mm).

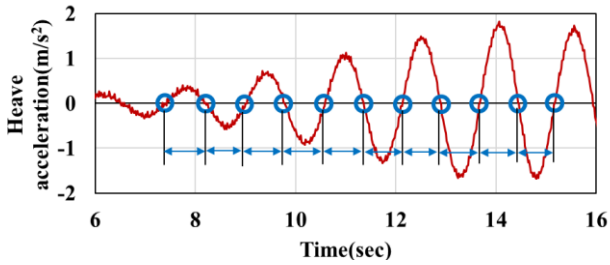

Figure 4.3 Transition of the periods of pitch and heave motions (ballast position = 20 mm).

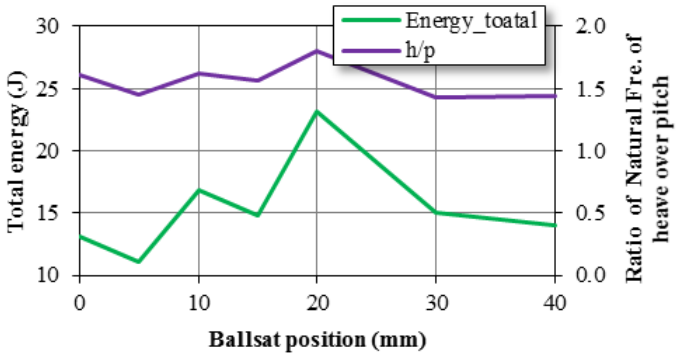

Figure 4.4 The total energy and frequency ratio between heave and pitch with ballast position changing.

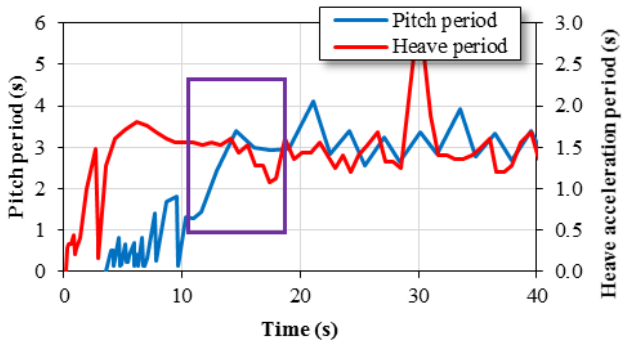

Figure 4.5 Transition of the periods of pitch and heave motions (ballast position = 0 mm).

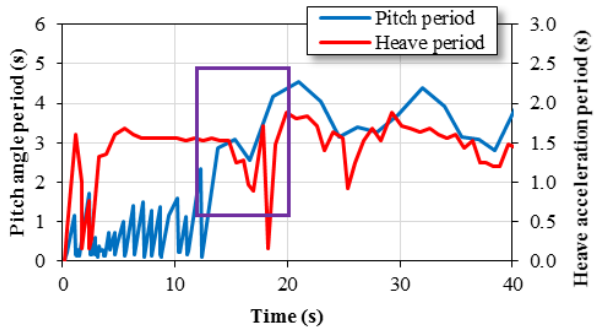

Figure 4.6 Transition of the periods of pitch and heave motions (ballast position = 20 mm).

4.4 Conclusion

The vertical velocities and displacements of the buoy were calculated based on the integration of signals of the heave acceleration. The kinetic energy of pitch and heave motions are calculated to investigate existence of the energy transform. The conclusion was obtained as follows： The total energy takes the maximum value around 16s and the first half of the peak is dominated by the heave energy and the latter half is replaced by the pitch energy. Therefore, this can be concluded that the energy was transferred from the heave mode to the pitch mode and shrunken by the pitch damping. On the other hand, the power to be taken off is closely related to the total energy.

Chapter5 Righting lever GZ analysis

5.1 Introduction

In order to find some conditions in which the large pitch motion occurs suddenly by considering the theoretical condition of the Mathieu-type instability. The righting lever of the buoy model is calculated with assuming the free board is infinite. The relationship between the pitch angle and the righting lever under the Mathieu-type instability was theoretically discussed in the time domain.

5.2 The righting lever GZ under the Mathieu-type instability condition

In order to understand the Mathieu-type instability in the time domain, the solution of Equation (2.41) is examined next. As is well known, the solution becomes unstable when $\omega_{nh}=2\omega n_{\varphi}$ and can be approximated by the following form.

$$\phi = Ce^{\left(\frac{S_\phi}{4\Delta_0 \overline{GM_0}\sqrt{1-\nu_\phi^2}}-\nu_\phi\right)\omega_{\phi n}t} \cdot \sin\left\{\omega_{\phi n}t + \frac{\theta_\zeta}{2}\right\} \tag{5.1}$$

where C is a constant to be determined by the initial conditions.

Therefore, looking at the exponential part of Equation (5.1), if the condition expressed by

$$S_\phi > 4\Delta_0 \overline{GM_0}\nu_\phi\sqrt{1-\nu_\phi^2} \tag{5.2}$$

is satisfied, the pitch amplitude becomes larger and larger as time proceeds.

Figure 5.1 shows the relationship between the pitch angle and the righting lever $GZ\ (=\overline{GM}(t)\cdot\phi(t))$ under the Mathieu-type instability expressed by Equation (5.1). The red arrows are added to the graph in order to indicate the movement of the relationship with the time progress. The ballast position was set to 20mm and the heaving amplitude z_0 was set to 15mm in the calculation. The relationship is plotted from t=0 to 15s. It can be observed that the pitch amplitude is increasing with time. Moreover, the righting lever takes larger value during the pitch motion is returning to the equilibrium position. It can be recognized as the physical explanation of the Mathieu-type instability in the time domain.

The righting lever of the buoy model is calculated with assuming the free board is infinite. Figure 5.2 denotes the calculated righting levers with respect to the draft. The GMs are also plotted in the figure as coloured lines. It can be shown that the righting lever GZ can be approximated by metacentric height GM as follows:

$$\overline{GZ(\theta,d)} \cong \overline{GM(d)}\cdot\phi \tag{5.3}$$

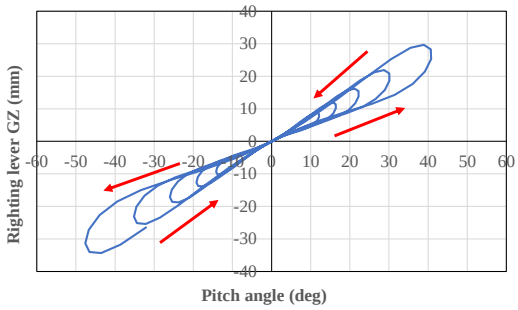

Figure 5.1 Relationship between the pitch angle and the righting lever GZ under the Mathieu-type instability condition. (t=0s~15s, z_0=15mm)

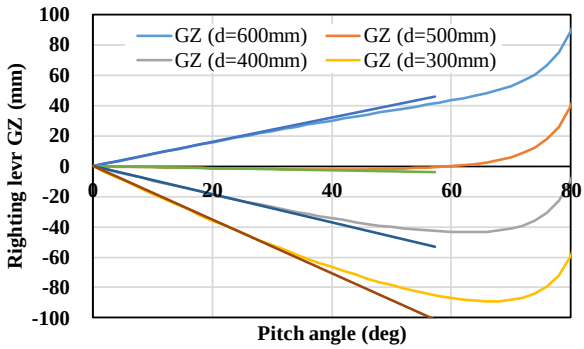

Figure 5.2 Righting levers GZ of the buoy model with respect to the draft (d=300mm~600mm).

5.3 The righting lever GZ under experiments

The experimental results shown in Figures 3.16 are investigated in the time domain. Figure 5.3a to 5.3f show the relationship between the pitch angle and the righting lever GZ with respect to the ballast positions 0, 5, 10, 20, 30 and 40mm. In the left figures, the green rectangles shows the samples time histories. In right figures, red arrows are also added to the graphs in order to indicate the movement of the relationship with the time progress. On the other hand, each blue arrow is indicating the last part of the large pitch motion. Compared to Figure 5.3, similar relationship can be seen in each figure. The larger righting levers can be seen when the pitch motion is returning to the equilibrium position. On the contrary, smaller righting levers, negative values in some cases, can be seen when the pitch motion is leaving from the equilibrium position. Furthermore, the inverse relationship can be seen at the end of the large pitch motion (at the blue arrow). This means that the large pitch motions disappear at the timing when the condition of the Mathieu-type instability is lost (righting levers become smaller when the pitch motion is returning to the equilibrium position).

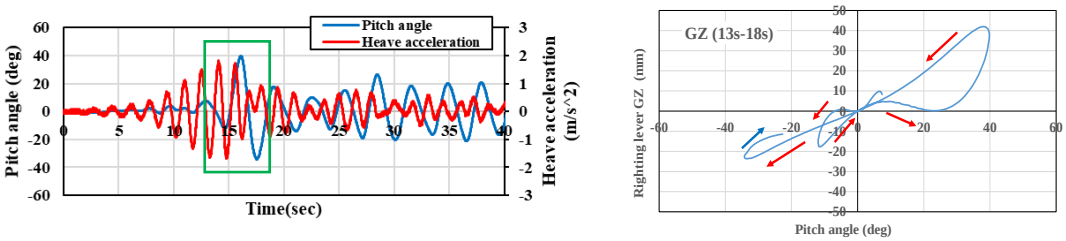

Figure 5.3a Relationship between the pitch angle and the righting lever GZ (right); Measured time histories of pitch angle and heave acceleration(left), see Figure 3.16a. (ballast position = 0 mm, t=13s~18s).

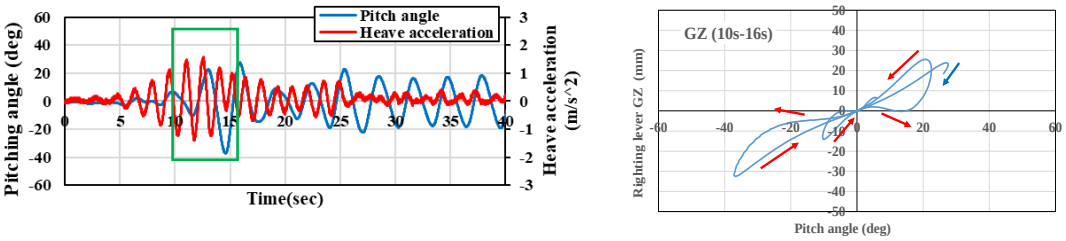

Figure 5.3b Relationship between the pitch angle and the righting lever GZ (right); Measured time histories of pitch angle and heave acceleration (left), see Figure 3.16b. (ballast position = 5 mm, t=10s~16s)

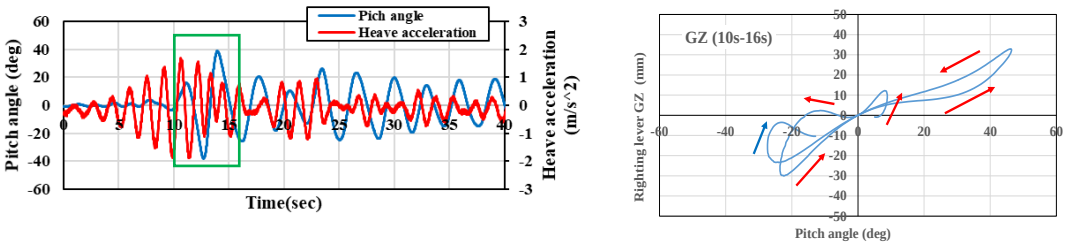

Figure 5.3c Relationship between the pitch angle and the righting lever GZ (right); Measured time histories of pitch angle and heave acceleration (left), see Figure 3.16c. (ballast position = 10 mm, t=10s~16s)

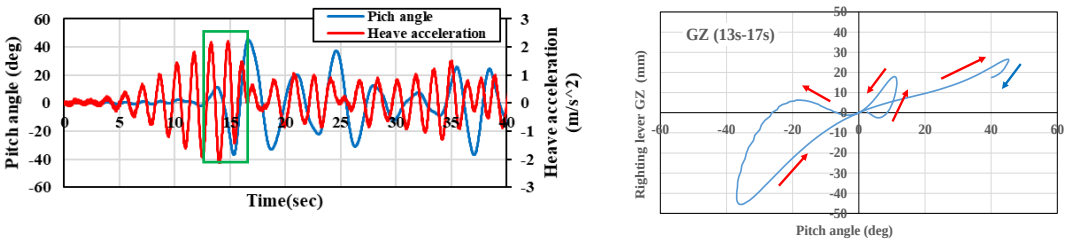

Figure 5.3d Relationship between the pitch angle and the righting lever GZ (right); Measured time histories of pitch angle and heave acceleration (left), see Figure 3.16d. (ballast position = 20 mm, t=13s~17s)

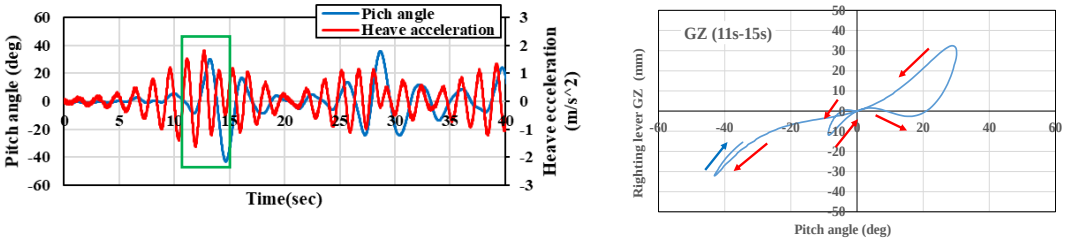

Figure 5.3e Relationship between the pitch angle and the righting lever GZ (right); Measured time histories of pitch angle and heave acceleration (left), see Figure 3.16e. (ballast position = 30 mm, t=11s~15s)

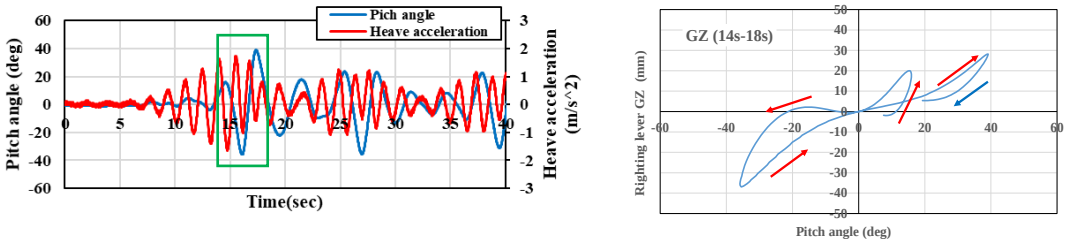

Figure 5.3f Relationship between the pitch angle and the righting lever GZ (right); Measured time histories of pitch angle and heave acceleration (left), see Figure 3.16f. (ballast position = 40 mm, t=14s~18s)

5.4 Conclusion

Based on the model experiments and considerations of the righting lever under Mathieu-type instability, the occurrence of the large pitch motion is discussed in the time domain. The results are summarized below:

(1) The righting lever of pitch motions can be changed by the draft (heaving motion).

(2) The relationship between the pitch angle and the righting lever under the Mathieu-type instability was theoretically discussed in the time domain.

(3) It was shown that the experimental relationship between the pitch angle and the righting lever during the large pitch motions is similar to the theoretical characteristic of the Mathieu-type instability.

(4) The large pitch motion disappears just after the theoretical characteristic of the Mathieu-type instability is lost.

Chapter6 Stability analysis of buoy motions

6.1 Introduction

In some experiments, it was observed that the large pitch motions became unstable and occurred suddenly. This unstable large pitch motion can produce much more kinetic energy and can be transformed to electricity, which is helpful for design the WECs and increase the generating efficiency. Hence, the corresponding peaks and troughs of pitch and heave motions are extracted out and the transient period was calculated. Based on the plotted stability charts of Mathieu equation, the occurrence of the large pitch motion was discussed with different ballast condition.

6.2 Stability analysis with experimental results

In this section, the measured experimental results in Figure 3.9 are investigated in the time history with the stability chart of the Mathieu equation. In order to analyse the phenomenon that the large pitch motions occurred suddenly at around 16 second, the corresponding peaks and troughs of pitch and heave motions are extracted out.

The time histories of transient periods in the vicinity intervals where the large pitch motion occurring are calculated by the time difference of the adjacent peaks or troughs. Figure 6.1 shows the measured partial time histories of pitch angle and heave acceleration with the ballast position at 0mm. The data of peaks and troughs in the vicinity of the large motions occurring are extracted to calculate the transient periods, and extracted times are defined as 'Time1' to 'Time10' (the circle marks in Figure (6.1). The same work is also applied to the ballast positions at 5mm, 10mm, 15mm and 20mm. The extracted times at different ballast positions keep the same characteristics as follows:

1）When the times locate at 'Time4'and 'Time5', the large pitch motions became unstable and the large pitch motion occurred suddenly;

2）After 'Time5', the pitch motions decayed, and the large pitch motions disappeared. After 'Time10', the large pitch motions occurred again.

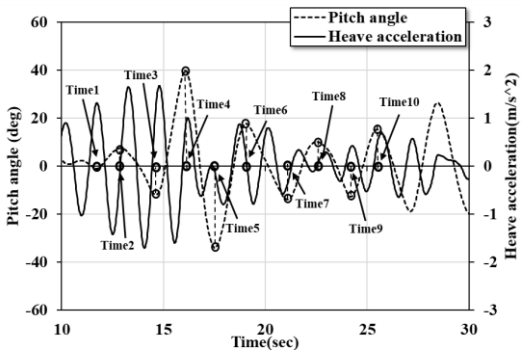

Figure 6.1 The extracted times in the time history of heave and pitch motions. (ballast position = 0mm)

In order to investigate these common characteristics of time histories of transient periods under experimental results, the transient frequencies of pitch and heave are assumed to be corresponding the natural frequency of pitch motion $\omega_{n\varphi}$ and the natural frequency of heave motion ω_{nh}.
The following equation is introduced again

$$\ddot{\phi}(t) + \{\delta + \varepsilon\, cos(\tau)\}\phi(t) = 0 \tag{6.1}$$

where the (δ, ε) can be obtained based on the equation of pitch motion shown in Equation (2.48).

$$\delta = \frac{\omega_{\varphi n}^2}{\omega_z^2}\left(1 - \nu_\phi^2\right),\ \varepsilon = \frac{\omega_{\varphi n}^2 S_\phi}{\omega_z^2}, \tau = \omega_z t + \theta_\zeta + \frac{\pi}{2} \tag{6.2}$$

The results of (δ, ε) are marked into the stability charts of Mathieu equation to perform the analysis. Here, δ is defined as concrete restoring coefficient and ε is defined as fluctuating restoring coefficient. Meanwhile, the amplitude of heave motion was assumed to be 0.1m in calculation for simplicity (the maximum amplitude of heave motions is about 0.1m in experiment results).

Figure 6.2a to 6.2e show the time histories (‘Time1’ to ‘Time10’) of the experimental results of (δ, ε) with different ballast positions in the stability charts of Mathieu equation. The arrows are added to the graph in order to indicate the movement of stability results with the time progress. The square marks of ‘Time1’ to ‘Time4’ are always in the unstable region, under the condition of which the pitch motion becomes unstable. It is also indicated that the large pitch motions occurred suddenly when that the times at ‘Time4’and ‘Time5’ (large pitch motions occur suddenly at around 15 second). It can be concluded that the large pitch motions can be induced when the condition of Mathieu-type instability in satisfied (the stability results of (δ, ε) is in unstable region). The first large pitch motion occurred until ‘Time5’, when at the time of which, it can be observed that all the results of stability are in the stable region with different ballast positions. The stability result of ‘Time5’ is marked by triangle marks. After ‘Time5’, it was shown in Figures 6.2 that all the large pitch motions disappeared (decayed) at a short time. And all the stability marks of ‘Time5’ are in the stable region (it is considered as that the condition of the Mathieu-type instability is lost at timing), which is the reason why pitch motion disappeared shortly just after the large pitch motion occurred. After large pitch motions disappeared (from ‘Time5’), all the stability marks of ‘Time6’ to ‘Time10’ return to the unstable region again, it is indicated that the large pitch motion occurred again, which is also indicated to be induced by the Mathieu-type instability.

The large pitch motions disappear (decayed) at the timing when the condition of the Mathieu-type instability is lost. Based on it, considering protecting the buoy device from damaging in the extreme weather, it is necessary to keep results of (δ, ε) always in stable region, which can reduce the overlarge pitch motion occurring. For example, the circle marks in Figures 6.2 are in the unstable

region, if there is enough inner space for ballast to move up and down and change the value of (δ, ε) to the stable region, for example, change value of (δ, ε) to the value of triangle marks, which can reduce the occurring of the large pitch motion to some extent.

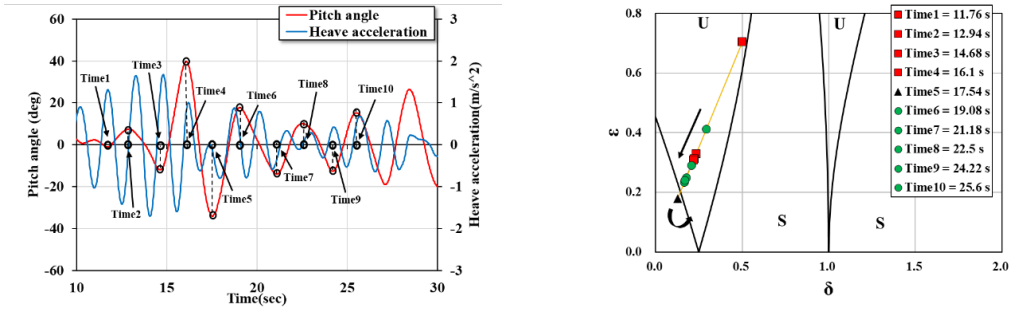

Figure 6.2a Stability analysis of buoy motions with experiment in time history (right); The extracted times in the repeated time history of heave and pitch motions (left). (ballast position = 0mm)

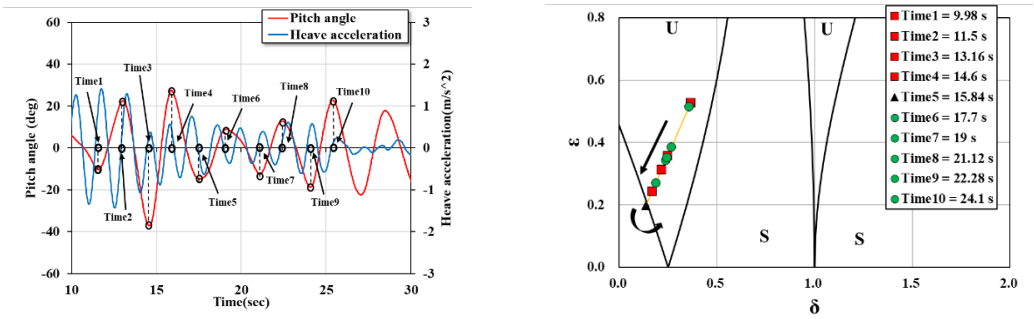

Figure 6.2b Stability analysis of buoy motions with experiment in time history (right); The extracted times in the repeated time history of heave and pitch motions (left). (ballast position = 5mm)

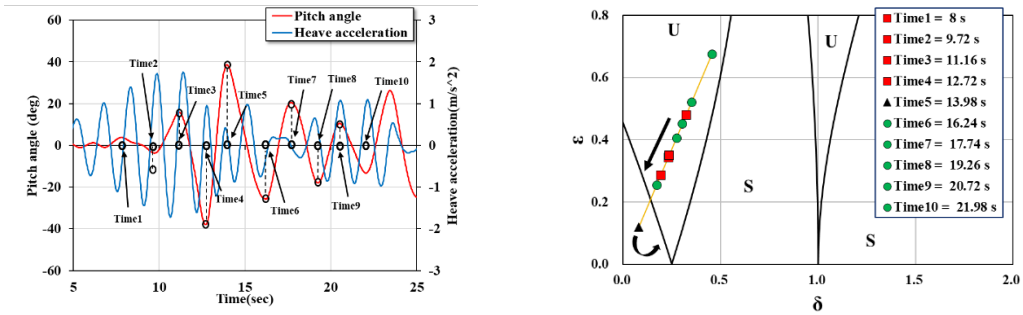

Figure 6.2c Stability analysis of buoy motions with experiment in time history (right); The extracted times in the repeated time history of heave and pitch motions (left). (ballast position = 10mm)

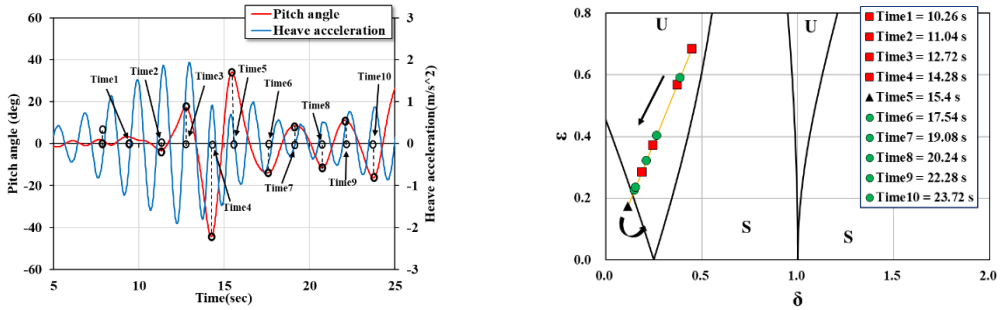

Figure 6.2d Stability analysis of buoy motions with experiment in time history (right); The extracted times in the repeated time history of heave and pitch motions (left). (ballast position = 15mm)

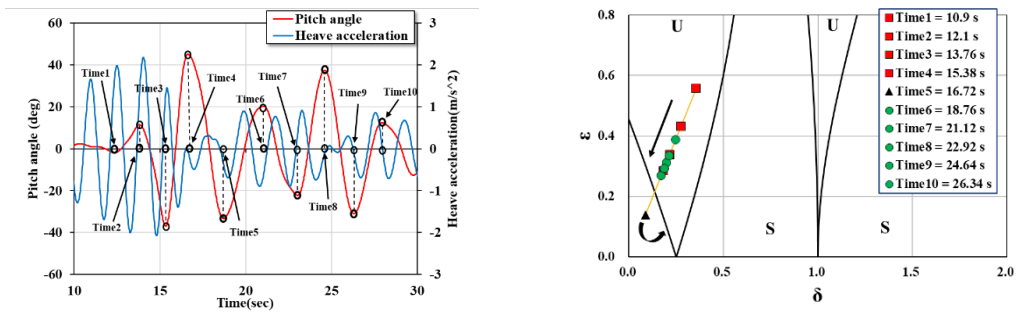

Figure 6.2e Stability analysis of buoy motions with experiment in time history (right); The extracted times in the repeated time history of heave and pitch motions (left). (ballast position = 20mm)

Based on the experimental results, as shown in Figure 6.3 and Figure 6.4, it is found that the large pitch motion occurred suddenly and the heave amplitude shrinks after the occurrence after large pitch occurring. The large kinetic energy is occurred just in the first time. The tendency of the total power will shrink with time progresses. The ballast positions in Figures are at 0mm and 40mm, other ballast positions also keep same above characteristics.

The main intention of the research is how to continue the tendency and keep large kinetic energy occur continuously. According to the previous conclusion, the large pitch motions disappearing at the timing is regarded as the buoy losing the condition of the Mathieu-type instability. In Equation 6.1 and 6.2, concrete restoring coefficient δ depends on the natural frequency of pitch motion ω_{np} and the natural frequency of heave motion ω_{nh}. From "Time4" to "Time5", it is found that the value of (δ, ε) is from unstable region to stable region, before which it is possible increase the natural frequency of pitch motion or decrease the natural frequency of the heave motion to be capable of keeping the value of (δ, ε) always in the unstable region. Then the large motion of buoy will occur continuously. In Figure 6.3and 6.4, Purple lines show the total

power of the large pitch motion occurring. Black lines show the power steady (average) without natural frequency controlling. The same calculations were carried out at different ballast positions. Compared with the no control of natural frequency, it is found that efficiency of kinetic energy will be improved up to 3-5 times with control. This is very useful to apply to the designment of WECs.

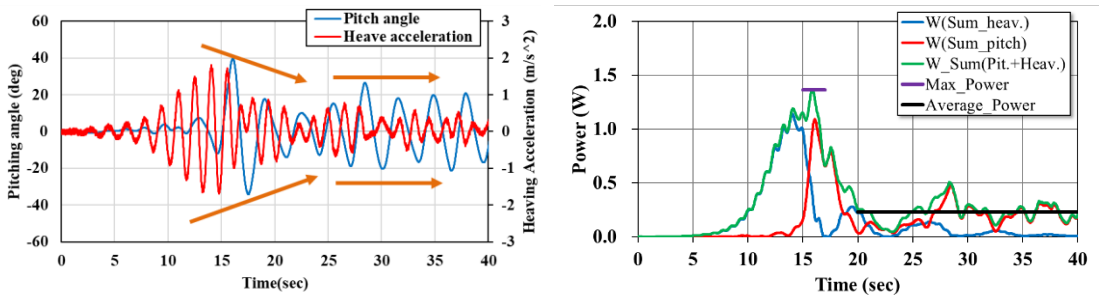

Figure 6.3 The energy time histories of the pitch angle and heave motion (right);
The time history of heave and pitch motions (right).
(ballast position = 0 mm)

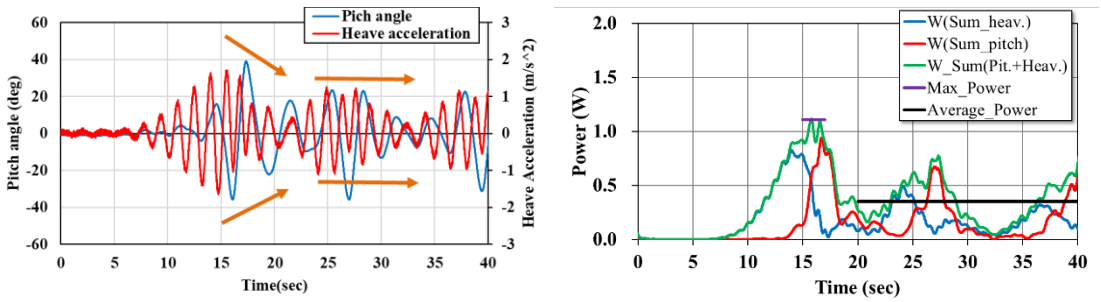

Figure 6.4 The energy time histories of the pitch angle and heave motion (right);
The time history of heave and pitch motions (right).
(ballast position = 40 mm)

6.3 Conclusion

In some experiments, it was observed that the large pitch motions became unstable and occurred suddenly. Based on the plotted stability charts of Mathieu equation, the occurrence of the large pitch motion was discussed. The results are summarized below:

(1) The stability chart of Mathieu equation was plotted for the experiment with the method of the harmonic balance.

(2) It could be found that all the experimental results of (δ, ε) were in the unstable region before the large pitch motion disappeared (until 'Time5'), which inducing the Mathieu-type instability of pitch motion.

(3) Before the large pitch motion decayed, that is at 'Time5', all the stability results were in the stable region of the stability chart of Mathieu equation.
(4) It has been indicated that the large pitch motions disappeared (decayed) at the timing when the condition of the Mathieu-type instability is lost.
(5) It has been shown stability results returned to the unstable region, and large pitch motion occurred again after large pitch motion disappeared, which is induced by the condition of Mathieu instability.

Chapter7 Conclusions and future research

7.1 Conclusions

Wave energy is an intermittent energy source, which is widely considered as one of the most alternative renewable and sustainable energy. WECs technologies are still in its infant stage, which naturally confronts this renewable energy converters with lots of challenges, problems and barriers during its maturation. To maximize the waves energy and realize the large oscillation of the buoy, the purpose of this research is to improve the efficiency by using parametric self-excited oscillation of WECs. The study focuses on the coupled motion of a spar-buoy type point absorber with coupled motions (heave and pitch), and the buoy is equipped with a ballast control system to generate parametric self-excited oscillation based on Mathieu-type instability. With using this buoy model, the measurement experiment was carried out in a regular wave. Using the system, the condition of the parametric pitch resonance phenomenon was investigated based on Mathieu-type instability. The results are summarized below:

(1) The large pitch motions occurred suddenly under the heave resonance condition. According to analyze the kinetic energy of the motions, it is indicated that the oscillation energy seems to be transferred from the heave mode to the pitch mode. Around the peak of the total energy occurring, the ratio of the natural frequencies between the heave and pitch motion almost equals 2. When the large pitch motion suddenly occurred, the phase relationship between the pitch angle and the heave acceleration showed the similar tendency with the theoretical Mathieu-type instability.

(2) The larger righting levers can be seen when the pitch motion is returning to the equilibrium position. On the contrary, smaller righting levers, negative values in some cases, can be seen when the pitch motion is leaving from the equilibrium position. Furthermore, the inverse relationship can be seen at the end of the large pitch motion. The large pitch motions occurred suddenly under the heave resonance condition. The righting lever of pitch motions can be changed by the draft (heaving motion). The relationship between the pitch angle and the righting lever under the Mathieu-type instability was theoretically discussed in the time domain. It was shown that the experimental relationship between the pitch angle and the righting lever during the large pitch motions is similar to the theoretical characteristic of the Mathieu-type instability. The large pitch motion disappears just after the theoretical characteristic of the Mathieu-type instability is lost.

(3) The stability chart of Mathieu equation was plotted for the experiment with the method of the harmonic balance. It could be found that all the experimental results of (δ, ε) (concrete restoring coefficient and fluctuating restoring force) were in the unstable region before the large pitch motion disappeared, which inducing the Mathieu-type instability of pitch motion. Before the large pitch motion decayed, all the stability results were in the stable region of the stability chart of Mathieu

equation. It has been indicated that the large pitch motions disappeared (decayed) at the timing when the condition of the Mathieu-type instability is lost. It has been shown stability results returned to the unstable region, and large pitch motion occurred again after large pitch motion disappeared, which is induced by the condition of Mathieu instability.

(4) Based on the parametrical oscillating characteristics, it is indicated that it is available how to utilize the dynamic frequency control for the WECs to realize the kinetic energy maximization, which is helpful for the WECs to harness the wave energy and transform to electricity. The main intention of the research is how to continue and keep large kinetic energy occur continuously. The large pitch motions disappearing at the timing is regarded as the buoy losing the condition of the Mathieu-type instability. The concrete restoring coefficient δ depends on the natural frequency of pitch motion ω_{np} and the natural frequency of heave motion ω_{nh}. Before Mathieu instability condition disappears, it is possible to increase the natural frequency of pitch motion or decrease the natural frequency of the heave motion in order to be capable of keeping the value of (δ, ε) always in the unstable region based on the stability chart of Mathieu equation. Then the large motion of buoy will occur continuously. The continuous large kinetic energy can improve the kinetic energy up to 3-5 times with frequency control, compared with the no control of natural frequency. This is very useful to be applied to the designment of WECs. The large kinetic energy can be transformed to the electricity. Power generation efficiency of renewable energy can be improved, which contributes to the development of human society.

7.2 Future work

The main contribution of this thesis is the construction of a new spar-type buoy model and parametric pitch resonance phenomenon was investigated based on Mathieu-type instability. However, for the sake of completeness, this model still requires some continued research:

- Power take-off (PTO) system

PTO system of WEC can absorb energy by the primary converter is transformed into useable electricity. The PTO system is essential as it will directly how efficiently the absorbed wave power is converted into electricity. Moreover, it also contributes to the mass, the size and the structural dynamics of the wave energy converter. PTO system will be introduced in the future experiment.

- The mooring system

Floating WECs need to have good power capture from the incident waves for most common frequencies. But floating bodies experience many external loads including winds, waves, and currents, which induced the point absorber drifting away from the desired location. The device should be moored using mooring systems. And the motions responding of the buoy under mooring system should be analyzed, especially make use of the theory of Mathieu instability.

- Numerical modeling

The Computational Fluid Dynamics (CFD) toolbox OpenFOAM will be used to perform numerical simulations of the point absorber wave energy converters (WECs) inside a numerical wave tank. The numerical and the experimental results for the WECs' motions will be investigated, it is not only helpful to simulate the motion response under different sea states, but also simplify the costly experimental investigation for WECs design.

Reference

[1] Lynn P A. Electricity from wave and tide: an introduction to marine energy[M]. John Wiley & Sons, 2013.

[2] Bilgen S, Kaygusuz K, Sari A. Renewable energy for a clean and sustainable future[J]. Energy sources, 2004, 26(12): 1119-1129.

[3] Van Der Ploeg F, Withagen C. Growth, renewables, and the optimal carbon tax[J]. International Economic Review, 2014, 55(1): 283-311.

[4] Solomon S, Qin D, Manning M, et al. IPCC fourth assessment report (AR4)[J]. Climate change, 2007.

[5] Solomon S, Manning M, Marquis M, et al. Climate change 2007-the physical science basis: Working group I contribution to the fourth assessment report of the IPCC[M]. Cambridge university press, 2007.

[6] Drew B, Plummer A R, Sahinkaya M N. A review of wave energy converter technology[J]. 2009.

[7] Ellabban O, Abu-Rub H, Blaabjerg F. Renewable energy resources: Current status, future prospects and their enabling technology[J]. Renewable and Sustainable Energy Reviews, 2014, 39: 748-764.

[8] Antonio F O. Wave energy utilization: A review of the technologies[J]. Renewable and sustainable energy reviews, 2010, 14(3): 899-918.

[9] Teske S, Muth J, Sawyer S, et al. Energy [r] evolution-a sustainable world energy outlook[M]. Greenpeace International, EREC and GWEC, 2012.

[10] J. Falnes, 2002 ‘ocean waves and oscillating systems’, Cambridge University Press.

[11] J. Falnes, 2007 ‘A review of wave-energy extraction’, Marine structure, Vol.20, pp185-201.

[12] Kalofotias F. Study for the Hull shape of a wave energy converter-point absorber; design optimization & modeling improvement[D]. University of Twente, 2016.

[13] Czech B, Bauer P. Wave energy converter concepts: Design challenges and classification[J]. IEEE Industrial Electronics Magazine, 2012, 6(2): 4-16.

[14] Heath T V. A review of oscillating water columns[J]. Philosophical Transactions of the Royal Society A: Mathematical, Physical and Engineering Sciences, 2012, 370(1959): 235-245.

[15] Charlier R H, Justus J R. Ocean energies: environmental, economic and technological aspects of alternative power sources[M]. Elsevier, 1993.

[16] Muetze A, Vining J G. Ocean wave energy conversion-a survey[C]//Conference record of the 2006 IEEE industry applications conference forty-first IAS annual meeting. IEEE, 2006, 3: 1410-1417.

[17] Karimirad M, Michailides C, Nematbakhsh A. Offshore Mechanics: Structural and Fluid Dynamics for Recent Applications[M]. John Wiley & Sons, 2018.

[18] Brekken T K A, Batten B A, Amon E A. From blue to green [ask the experts][J]. IEEE Control

Systems Magazine, 2011, 31(5): 18-24.
[19] Clément A, McCullen P, Falcão A, et al. Wave energy in Europe: current status and perspectives[J]. Renewable and sustainable energy reviews, 2002, 6(5): 405-431.
[20] Lejerskog E, Gravråkmo H, Savin A, et al. Lysekil research site, sweden: A status update[C]//9th European Wave and Tidal Energy Conference, Southampton, UK, 5-9 September 2011. 2011.
[21] Improvement M, Kalofotias F. Study for the Hull Shape of a Wave Energy Converter-Point Absorber[J]. 2016.
[22] Falnes J. Optimum control of oscillation of wave-energy converters[J]. International Journal of Offshore and Polar Engineering, 2002, 12(02).
[23] Falnes, J. and Budal, K., 1978, “Wave-power conversion by power absorbers, Norwegian Maritime Research 6 (4), 2-11.
[24] Budal, K. and Falnes, J., 1980, “Interacting point absorbers with controlled motion”, in: B. Count (Ed.), Power form the Waves, Academic Press, London, 381-399.
[25] Eidsmoen H. Tight-moored amplitude-limited heaving-buoy wave-energy converter with phase control[J]. Applied Ocean Research, 1998, 20(3): 157-161.
[26] António F O. Phase control through load control of oscillating-body wave energy converters with hydraulic PTO system[J]. Ocean Engineering, 2008, 35(3-4): 358-366.
[27] Eidsmoen H. Simulation of a slack-moored heaving-buoy wave-energy converter with phase control[J]. 1996.
[28] Falnes J. Principles for capture of energy from ocean waves. Phase control and optimum oscillation[J]. Department of Physics, NTNU, N-7034 Trondheim, Norway, 1997: 1-8.
[29] Shek J K H, Macpherson D E, Mueller M A. Phase and amplitude control of a linear generator for wave energy conversion[J]. 2008.
[30] Babarit A, Clément A H. Optimal latching control of a wave energy device in regular and irregular waves[J]. Applied Ocean Research, 2006, 28(2): 77-91.
[31] Babarit A, Duclos G, Clément A H. Comparison of latching control strategies for a heaving wave energy device in random sea[J]. Applied Ocean Research, 2004, 26(5): 227-238.
[32] Henriques J C C, Lopes M F P, Gomes R P F, et al. On the annual wave energy absorption by two-body heaving WECs with latching control[J]. Renewable Energy, 2012, 45: 31-40.
[33] Sheng W, Alcorn R, Lewis A. On improving wave energy conversion, part I: Optimal and control technologies[J]. Renewable Energy, 2015, 75: 922-934.
[34] Koo B J, Kim M H, Randall R E. Mathieu instability of a spar platform with mooring and risers[J]. Ocean engineering, 2004, 31(17-18): 2175-2208.
[35] Iseki T. Optimization Method for Oscillation Characteristics of a Spar-Buoy[C]//ASME 2014 33rd International Conference on Ocean, Offshore and Arctic Engineering. American Society of Mechanical

Engineers Digital Collection, 2014.

[36] Rho J B, Choi H S, Shin H S, et al. Heave and pitch motions of a spar platform with damping plate[C]//The Twelfth International Offshore and Polar Engineering Conference. International Society of Offshore and Polar Engineers, 2002.

[37] Haslum H A, Faltinsen O M. Alternative shape of spar platforms for use in hostile areas[C]//Offshore technology conference. Offshore Technology Conference, 1999.

[38] ZHAO J, TANG Y, WANG W. Study on the parametrically excited mathieu instability of a classic spar platform[J]. Engineering Mechanics, 2010, 3.

[39] Yong-Pyo H, Dong-Yeon L, Yong-Ho C, et al. An experimental study on the extreme motion responses of a spar platform in the heave resonant waves[C]//The Fifteenth International Offshore and Polar Engineering Conference. International Society of Offshore and Polar Engineers, 2005.

[40] Iseki T. Optimization Method for Oscillation Characteristics of a Spar-Buoy[C]//ASME 2014 33rd International Conference on Ocean, Offshore and Arctic Engineering. American Society of Mechanical Engineers Digital Collection, 2014.

[41] Iseki T. Dynamic control of oscillation characteristics of a spar-buoy[M]//Maritime Technology and Engineering. CRC Press, 2014: 1257-1264.

[42] Iseki T. Experimental Study on Dynamic Control of Oscillation Characteristics of a Spar-Buoy[C]//ASME 2017 36th International Conference on Ocean, Offshore and Arctic Engineering. American Society of Mechanical Engineers Digital Collection, 2017.

[43] XU, PENG and Iseki, T., 2018, “Experimental Study on Oscillation Characteristics of a Spar-buoy under Mathieu Instability”, Proceedings of 3rd International Conference on Offshore Renewable Energy (CORE 2018), 2, 170-178.

[44] Iseki, T. and XU PENG, 2019, “Experimental Study on coupled motions of a spar-buoy under Mathieu instability”, Proc. OMAE2019-95937.

[45] XU, PENG and Iseki, T., 2020, “Experimental Study on Parametrically Excited Oscillation of a Spar-Buoy Under Mathieu Instability”, Journal of the Japan society of naval architects and ocean engineers, 30, 97-103.

[46] Van der Pol, B. and Strutt, M. J. O., 1928, “On the stability of the solutions of Mathieu’s equation”, Phil. Mag. J. Sci. 5, 18-38.

[47] Kovacic I, Rand R, Sah S M. Mathieu's Equation and Its Generalizations: Overview of Stability Charts and Their Features[J]. Applied Mechanics Reviews, 2018, 70(2): 02080.

Acknowledge

Firstly, I would like to express heartfelt gratitude to my supervisor Prof. Iseki Toshio for the continuous encouragement and support of my Ph.D. research, for his instructive advice and valuable suggestions on this thesis. He deserves more respect and my appreciation for his dedication to academic research and his kindness. His immense knowledge and enthusiasm at work have always been great motivation and tremendous encouragement to me. I have learnt a lot from him and his enthusiasm and support have made working in his lab a wonderful learning experience.

My research work is also supervised by Prof. Minami and Prof. Okazaki. I express sincere gratitude to them.

My research work is partly supported by the Sasakawa Scientific Research Grant from The Japan Science Society. This work is also supported by JSPS KAKENHI Grant Number 17K06960. I express sincere gratitude to the organizations.

I would like to express gratitude to Miss Hong, Miss Sekine, Mr Duan Liangliang, Mr Tsuchiya and Mr Yamashita, who gave much help during my experiment and life in Japan.

I would also like to thank my Chinese friends, who sent video calls or messages to comfort me in some depressed moments.

Last but not least, special thanks to my family, who have been helping me out of difficulties and supporting without a word of complaint.

XU PENG
March 2020
Tokyo, Japan

List of publications

［1］ XU, PENG and Iseki, T., 2018, “Experimental Study on Oscillation Characteristics of a Spar-buoy under Mathieu Instability”, Proceedings of 3rd International Conference on Offshore Renewable Energy (CORE 2018), 2, 170-178.

［2］ Iseki, T. and XU PENG, 2019, “Experimental Study on coupled motions of a spar-buoy under Mathieu instability”, Proc. OMAE2019-95937.

［3］ XU, PENG and Iseki, T., 2019, “Experimental Study on Parametrically Excited Oscillation of a Spar-Buoy Under Mathieu Instability” [J], Journal of the Japan society of naval architects and ocean engineers, 30，97-103.

[4]日本船舶海洋工学会，2018 年 6 月，“スパー型ブイのパラメトリック励振について”（発表）

[5]2018 年度日本笹川科学研究発表会，2019 年 4 月，“波力発電におけるパラメトリック励振の利用に関する実験的研究”（発表）